Tracking metal pathways in magmas using volcanic gas fingerprints

Marie Edmonds[1]*, Tamsin A. Mather[2], Emma J. Liu[1]

1. Department of Earth Sciences, University of Cambridge, Downing Street, Cambridge CB2 3EQ
2. Department of Earth Sciences, University of Oxford, S Parks Rd, Oxford OX1 3AN

* corresponding author

As well as gases that regulate climate over geological time, volcanoes emit prodigious quantities of metals into the atmosphere, where they have key roles as catalysts, pollutants and nutrients. Here we compare arc basaltic volcano metal emissions measurements to those from hotspot settings. As well as emitting higher fluxes of metals (similar to those building ore deposits), these arc emissions possess a distinct compositional fingerprint, particularly rich in tungsten, arsenic, thallium, antimony and lead compared to those from hotspots. We propose volcanic metal emissions are controlled by magmatic water content and redox: hydrous arc magmas that do not undergo sulfide saturation yield metal-rich, saline aqueous fluid; shallow degassing and resorption of late-stage sulfides feeds volcanic gases at Hawai'i and Iceland. While global arc magma chemistries vary significantly, our findings suggest that volcanic emissions in arcs have a distinct fingerprint compared to other settings. A shift in global volcanic metal emissions may have occurred in Earth's past as more oxidized, water-rich magmas became prevalent, influencing the surface environment.

An important, yet poorly quantified, part of the solid Earth metal cycle is the transport of dissolved metals by magmas, followed by their sequestration as crustal ore deposits or

outgassing into the surface environment during volcanic eruptions. Metals play key roles in a number of Earth processes. The flux of volcanically-mediated metals from submarine arc volcanoes into past euxinic oceans[1] may have been of key importance for the evolution of life. Transition metals outgassed by volcanoes catalyse the aqueous oxidation of sulfur[2]. Magmatic aqueous fluid is an important medium for transporting metals to sites of ore deposits[3,4]. With some notable exceptions, studies of volcanic metal emissions have been dominated by studies of condensates from low temperature fumaroles[5], generated during shallow cooling of magmatic fluids. These fluids are generally metal-poor, owing to their low temperature (below most gaseous metal condensation temperatures) and low salinity at low pressures[3]. There are a number of datasets from the plumes of active basaltic volcanoes[6-10] however, which show that these volcanoes are emitting fluxes of metals[6,8,11,12] of similar scale to those from large industrial smelters[13] and those building crustal ore deposits[3,6], making basaltic volcanoes a significant source of metals (and semi-metals) into the atmosphere and oceans. Studying basaltic volcanic systems, instead of their more evolved counterparts, brings advantages: high metal fluxes, safer sampling, a magma less affected by differentiation (and consequent metal fractionation) and a style of volcanism more representative of that prevalent on early Earth, possibly providing insights into metal fluxing into the early ocean and atmosphere. It is expected, from metal ratios in ore deposits[14] and sulfides[15] and metal systematics in glasses[16,17] that mid-ocean ridge, hotspot and arc basaltic volcanoes should have different assemblages of outgassing metals. This has been noted by previous studies[9,18], but a systematic explanation for these differences has been lacking, until now.

Metal outputs of basaltic volcanoes into the atmosphere

Figure 1 presents a compilation of volcanic gas and aerosol metal data[6-10,12] (**Supplementary Material**) acquired at six active, basaltic volcanoes in a range of tectonic settings. Cu, Tl, Cd,

Zn, Pb, Se and Sn fluxes into the atmosphere can reach 10^3-10^4 kg/day at basaltic arc volcanoes and fluxes of a number of other metals (e.g., In) and semi-metals (Bi, As) can exceed 100 kg/day (**figure 1A**), similar to metal fluxes involved in crustal ore deposit development[3]. Metal fluxes from hotspot volcanoes Kīlauea (Hawai`i, USA; during the 2008-2018 summit eruption) and Holuhraun (Iceland; during the 2014-2015 eruption) are lower, not exceeding 100 kg/day for any metal/semi-metal species (although upper error limits for Zn and Se exceed this). Further, the data in **figure 1A** indicate that the metal composition of volcanic emissions differs systematically between arc and hotspot settings. The emissions from Kīlauea and Holuhraun aerosols are dominated by Se, Cd, Te, Pb, Cu and Zn and there are markedly lower fluxes of W, In, As, Cs and Tl over arc volcanic aerosols. Arc volcanic aerosols, in contrast, have the highest fluxes of Pb, Cu, Zn, Tl, As, Sn, Se. The minor silicate contributions to most of the key elements In, As, Cs and Tl inferred from the data from Stromboli, Masaya, Etna and Ambrym (**Supplementary Material**) mean that a variable silicate ash fraction of the plumes is unlikely to account for these differences[6,7,36]. Further, the plume metal compositions do not mirror the composition of the lavas (**figure 1B**), which suggests that the gas compositions are not merely controlled by the initial compositions of the magmas in the different tectonic settings, although it is important to note that another recent study documented enrichments in Sb, As, Tl, W and Pb in Manus Basin submarine arc basalts over MORB[19]. Arc lavas (here exemplified by Stromboli and Etna) are, overall, richer in metals such as Sb, U, Te, W, Cs, but are not appreciably richer in the other metal species, in particular those which are so abundant in the plume, e.g., Pb, Cu, Sn and Zn. In fact, Cu, Sn and Zn have similar concentrations in erupted lavas from all of the volcanoes, even when degassing is accounted for (dashed lines in **figure 1B** show pre-degassing metal concentrations). The absolute flux of metals for a particular volcano is controlled by magma degassing rate and style of volcanic activity, which would elevate or depress metal fluxes, but

76 is not expected to change the distinctive patterns observed in the relative metal abundances
77 shown in **figure 1A**. The ratios X/SO_2, where X is a metal (or semi-metal), also show
78 differences between settings (**Supplementary Material**), with X/SO_2 being generally lower
79 for the hotspot volcanoes ($<1 \times 10^{-4}$ for most metals and semi-metals, with many $<1 \times 10^{-6}$),
80 extending up to 1×10^{-3} for Pb, Zn and Cu for the arc volcanoes.
81
82 We propose that the metals measured in these volcanic plumes were transported in the
83 exsolved magmatic volatile phase prior to and during eruption. A plot of enrichment factors
84 (see **methods**) demonstrates the tendency of the metals to exist in the volcanic plume gas and
85 aerosol phase over the silicate melt phase, relative to Cu (**figure 1C**). Enrichment factors
86 reach overall higher values for the hotspot volcanic systems: greater than 10^2 for In, Bi and
87 Cd (for both Kīlauea and Holuhraun) and As, Tl and Pb (for Holuhraun) and reaching 10^4-10^5
88 for Te and Se, the most volatile semi-metals. For the arc plumes, enrichment factors are in
89 general lower but follow the same overall trends (**figure 1C**). Te, Se, Cd and Bi exhibit much
90 lower enrichment factors referenced to Cu in high-temperature these arc volcanic gases over
91 hotspot volcanic gases, despite similar or higher concentrations of these metals in the melt
92 prior to degassing (**figure 1B**). Kinetic effects may be important under certain conditions; it
93 has been shown that significant variation in, e.g., Tl/Pb is possible in silicate melt during
94 degassing, due to diffusive fractionation[20]. These effects are poorly understood yet unlikely to
95 explain the order of magnitude differences observed in Tl/Pb here (**figure 1A**).
96
97 **Metal pathways in magmas prior to eruption**
98 Explaining the systematic differences in trace metal emissions between these arc and hotspot
99 volcanoes requires consideration of the processes that partition metals during magma ascent
100 and eruption. In magmatic systems in the crust, metals partition between silicate melt, an

aqueous fluid phase (which may be a hypercritical phase or an aqueous liquid at mid-crustal pressures, or a vapor phase at low pressures, comprising CO_2, water, sulfur and halogen species), and a sulfide phase (liquid sulfide, or monosulfide solid solution, depending on temperature), should they be present. Other phases, such as silicates, oxides and phosphates, may also take up metals, but are of subordinate importance. Both chalcophile and siderophile metals partition strongly into both aqueous fluid and sulfide phases over silicate melt over a range of temperatures and pressures. Aqueous fluid-melt partition coefficients are constant regardless of whether a sulfide phase is present; therefore the presence of sulfide sequesters metals such that both the melt and aqueous fluid phases become metal-depleted. Many experimental determinations of metal partitioning have been under conditions not directly relevant to volatile-rich magmas in the crust, e.g., at mantle pressures [21,22]. Little attention has been paid to those metals most prevalent in volcanic gases, such as Zn, Sn, Pb and Tl. Experiments at ~200 MPa on andesites and basalts with co-existing sulfide, silicate melt and aqueous fluid[23-26] show that aqueous fluid-melt partitioning is dependent on the composition of the aqueous fluid and on redox. High Au concentrations in silicate melt are promoted by conditions just below the sulfide-sulfate transition (which is gradual and occurs ~NNO+0.5)[23]. The fluid-melt partitioning of Au is enhanced at fO_2 <NNO+0.5 and suppressed at higher fO_2 and when SO_2 dominates the aqueous fluid phase, in contrast to the partitioning of Cu, which is much less dependent on S speciation[26]. A recent set of experiments on aqueous fluid-melt partitioning of a wide range of metals in mafic magma, in the presence of S- and Cl-bearing aqueous fluid (**Supplementary Material Table 2**), showed that Cu, Se, Te and Cd are most volatile, followed by Zn, As, Ag, Sb, Cs, W, Tl, and Bi[24]. This is broadly consistent with the volcanic emissions measurements shown in **Figure 1C** although W, Cs and Zn show lower enrichment factors compared to Cu than these experiments might predict.

126

127 To understand the balance between the silicate melt-aqueous fluid and silicate melt-sulfide
128 partitioning further, a compilation of sulfide-silicate melt, and vapor-melt partition
129 coefficients for metals is shown in **figure 2** (citations and experimental conditions in
130 **Supplementary Material**). Also shown in **figure 2** are the calculated emanation coefficients
131 (see **methods**) of the metals (and semi-metals) in the gas/aerosol plumes of the basaltic
132 volcanoes, plotted in order of the Holuhraun data. These data show that the hotspot basaltic
133 volcanic emissions plumes (Kīlauea and Holuhraun) are particularly poor in those metals that
134 partition more strongly into aqueous saline fluid than the sulfide phase, such as U, Cs, W, Zn,
135 Mo (left hand side of the plot). The plumes from Kīlauea and Holuhraun are particularly rich
136 (with emanation coefficients of 1–100%) in those metals and semi-metals which partition
137 strongly into sulfide over silicate melt (with partition coefficients of >100; on the right-hand
138 side of the plot), such as Cd, Se, Te (no data exists for Au in the gas plumes of Kīlauea or
139 Holuhraun; **Figure 2**). In contrast, the data for these arc gases show that all metals have an
140 emanation coefficient of >0.1% (with the exception of U for Stromboli). These arc plumes are
141 richer in U, Cs, W, Cu than hotspot volcanic plumes; these elements are associated with
142 significantly higher aqueous fluid-melt partition coefficients (up to 10^1–10^2; note the aqueous
143 fluid-melt partition coefficient for Sn is for rhyolite melt[27] and the partition coefficient
144 increases with the chlorine content of the aqueous fluid[27]) relative to their sulfide-silicate melt
145 partition coefficients (<10, with the exception of Cu).
146

147 **Effect of the timing of aqueous fluid and sulfide saturation**

148 Arc basalts contain, on average, 4 wt% H_2O[29], and 0.5–2.0 wt% CO_2[30]. Aqueous fluid
149 saturation is expected to occur in the mid-crust, into which metals will partition, strongly in
150 some cases (**figure 2**). Hotspot basalts, in contrast, contain 0.5-1.0 wt% H_2O[31] and 0.5 to 1.0

151 wt% CO_2[32], which results in the exsolved fluid becoming water-rich only at shallower depths.
152 Importantly, the fluid phase will be strongly CO_2-dominated until the magma reaches low
153 pressures (<100 MPa) during magma ascent, when H_2O and sulfur (as H_2S or SO_2) partition
154 into the aqueous vapor phase[33,34]. The metal-carrying capacity of CO_2-rich aqueous fluid has
155 been shown to be poor[35].
156
157 Models of sulfide saturation[36,37] show that while mid-ocean ridge basalts are likely saturated
158 in sulfide on eruption, more oxidized basalts, where a greater proportion of sulfur is present as
159 sulfate[38,39], must fractionate to a greater degree to achieve sulfide saturation. Some basalts
160 may not saturate in sulfide at all[39,40]. Sulfides are not commonly present (as quenched sulfide
161 liquid or sulfide minerals), either in the groundmass or as inclusions, in the erupted products
162 of Stromboli, Etna and Ambrym[41]. In contrast 2014–2015 Holuhraun Icelandic melts contain
163 abundant sulfides on eruption; as do the matrix glass and melt inclusions of Laki[42]. At
164 Kīlauea, basaltic tephra contain sulfides as inclusions in olivine. Sulfur systematics in the
165 matrix glasses of basalts from Iceland and Kīlauea are consistent with sulfide saturation on or
166 shortly before eruption[43].
167
168 If sulfide saturates prior to an aqueous fluid in the deep crust (**figure 3, middle**), dense
169 sulfides may be sequestered into cumulates, thus removing metals from the silicate-melt
170 aqueous fluid system and generating chalcophile-poor melt (and aqueous fluid) upon further
171 ascent and eruption of the magma; this has been suggested as an explanation for the lack of
172 ore deposits in relatively water-poor 'barren' arc magmatic systems[44]. A chalcophile-poor arc
173 volcanic gas is not a feature of the datasets presented here. If, however, an aqueous fluid
174 phase forms before sulfide saturation, which is likely for a water-rich arc basalt (**figure 3,**
175 **right**), metals will partition strongly into the saline aqueous fluid[45]. If the silicate melt does

176 not saturate with sulfide[16], the aqueous fluid will remain metal-rich and will be outgassed
177 during magma ascent and eruption at the surface with the metals in proportions controlled by
178 their respective fluid-melt partition coefficients. If the melts are very chlorine-rich, a brine
179 phase may form at low pressure, unmixing, along with a low density vapor, from a
180 supercritical fluid described by the solvus in the NaCl-H_2O system[3]. Brine formation may
181 fractionate metals; however these effects are minimal for basalts degassing near atmospheric
182 pressure, which are relatively poor in chlorine (compared to rhyolites) and are likely to
183 transport a saline aqueous fluid phase up to the surface (including any minor brine phase)[3].
184 The vapor phase in the sulfide-free case will then be rich in a range of fluid-mobile
185 metals/semi-metals, just as observed in the arc volcanic gas data presented here (**figure 1**).
186 Note that primary melts in arc settings may also be variably enriched in fluid-mobile metals[19],
187 caused by fluid addition to the mantle wedge directly from the slab. However, the data
188 presented here suggest that further partitioning into the aqueous fluid phase must also take
189 place to explain the enrichment in fluid-mobile metals in the volcanic emissions over the
190 silicate melt (**figures 1B, 2**).
191
192 If sulfide saturates after an aqueous fluid phase, the sulfides may play some role in metal
193 partitioning during shallow eruption and degassing processes. The hotspot volcanic gases in
194 **figure 1A** are rich in chalcophiles (e.g., Cd, Te, Se) and the emanation coefficients of the
195 gases in these plumes broadly follows sulfide-silicate melt partition coefficients (**figure 2**),
196 suggesting that metals are sourced from sulfides directly, either via a mantle melting process[46]
197 or through the formation of a sulfide liquid droplet at the interface between a silicate melt and
198 aqueous fluid bubble[47,48], shown as "vapor-sulfide aggregates", in **Figure 3** (**left**). Sulfides
199 may become unstable due to oxidation during attachment to a vapor bubble and may then be
200 resorbed during exsolution of an aqueous vapor phase[49]. In this way, metals that were bound

201 in sulfides[17] are released to the silicate melt-vapor system, and then to the atmosphere.
202 Congruent dissolution of sulfides within these bubble-sulfide aggregates has been proposed to
203 explain the similarity of metal outgassing ratios to metal ratios in sulfides at some
204 volcanoes[47,50].
205
206 **Implications of systematic volcanic metal emissions variations**
207 The four arc volcanoes presented here have a distinctive metal outgassing fingerprint, with
208 higher concentrations of Cs, As, In, W and Tl over hotspot volcanoes (**Figure 1**). While
209 global arc magma chemistries vary significantly, we propose that these characteristic metal
210 enrichments will be a broad feature of global arc volcanic plumes due to their relatively
211 oxidized nature, low degree of fractional crystallization and high magma water and chlorine
212 contents. Together, these factors suppress sulfide saturation promoting partitioning of
213 metals/semi-metal directly into aqueous/saline aqueous fluid rather than metal/semi-metal
214 degassing being mediated by sulfides (**Figure 3**).
215
216 Saline aqueous fluids clearly play an important role in transporting large fluxes of metals
217 from basaltic melts through the mid and upper crust, eventually either outgassing from
218 volcanoes or being incorporated into ore deposits. Volcanic outgassing of metals and ore
219 deposit formation may be effectively mutually exclusive in any particularly time period. In
220 fact, the gases emitted from volcanoes are representative of the fluids that, under different
221 conditions of magma supply or tectonic stress, might instead precipitate economically viable
222 concentrations of metals and sulfur in shallow crustal porphyries. In arc magmatic systems,
223 there is good evidence that mafic magmas of the type that we observe outgassing at the
224 surface (**figure 1**) underplate felsic magmas in the crust[53]. Recharging mafic magmas clearly
225 have potential to supply extensive fluxes of volatiles to overlying felsic magmas via an

aqueous fluid phase which might migrate efficiently through crystal-rich, near-solidus magmas[54,55]. Accumulation of aqueous fluid at the roof zones of such reservoirs may therefore trigger the shallow intrusion of stocks and then be the medium from which metals are precipitated in copper porphyry systems[3], without the need to invoke reworking of magmatic sulfides to concentrate metals.

There may be broader implications of the important role of volcanoes in metal geochemical cycling. It has been proposed that arc basalts were not oxidized until the late Neoproterozoic, when extensive ocean bottom water sulfate led to subducted sulfate oxidizing the sub-arc mantle[56], which coincides with copper and gold porphyries becoming prominent in the geological record[56,57]. Submarine arc volcanoes during the Archaean and much of the Proterozoic may hence have outgassed mixtures of metals very much like hotspot volcanoes today; with higher volcanic arc outgassing fluxes of W, Cs, As, Tl, Pb, Cu and Zn (similar to modern arc volcanoes) only becoming widespread in the earliest Phanerozoic, when shallow submarine arc vents may have become significant localized sources of these biologically important metals in the ocean[58].

Methods

Enrichment factors were calculated by normalizing gas plume metal concentrations by Cu concentrations, and lava metal compositions by Cu concentrations and then dividing the former by the latter. This normalization step is necessary because plume dilution is variable between datasets. Enrichment factor (EF) is then a quantity that is comparable between sources and is given by:

$$EF_{Cu} = \frac{\left(\frac{[X]}{[Cu]}\right)_{gas}}{\left(\frac{[X]}{[Cu]}\right)_{lava}} \quad (1)$$

We have used Cu as our normalizing element, rather than a more lithophile element such as a REE or Al, Mg, because the latter necessitates accounting far more accurately for the contamination of the samples by silicate material. Cu has been affected by contamination by ash, but only by up to 6%; see **supplementary material** for discussion). Cu is a poorly to moderately volatile element, which is reflected in the plot of enrichment factors; most metals plot at higher values than Cu. EF<1 means the element is less "volatile" than Cu; EF>1 means the element is more "volatile" than Cu. Ours is not the first study to use a moderately volatile element to normalize data to generate EF; Br has been used in several studies[6].

The emanation coefficient, ε_x, is calculated as the percentage of the metal *x* that has degassed from the silicate melt, equal to:

$$\varepsilon_x = \left(c_i - c_f\right) \Big/ c_i \qquad (2)$$

where c_i is the initial concentration of element x in the magma and c_f is the final concentration of element *x* in the post-eruptive lava (as originally defined by [59], who used this relation to describe the degassing of radionuclides ^{222}Rn, ^{210}Po, ^{210}Bi and ^{210}Pb).

We use two methods to calculate emanation coefficients shown in **Figure 2** (see Supplementary Material Table 1). The emanation coefficient ε_x of these elements from the magma can be assessed from their mean enrichment factor (EF, see equation 1 above) and the emanation coefficient of Pb from molten basalt (which we assume to be constant at 0.01[60]), as[6,8,61]:

$$\varepsilon_x^{-1} = 1 + \left[\left(EF_{Pb} \Big/ EF_x \right) \left(1 - \varepsilon_{Pb}\right) \Big/ \varepsilon_{Pb} \right] \qquad (3)$$

We also calculate the concentration of metals and semi-metals in the silicate melt prior to degassing and then the emanation coefficient using equation 2 above. The amount of metal (or semi-metal) in the gas plume was "added" back into to the degassed lava composition by converting the mass X/SO_2 ratio in the plume (**Supplementary Material figure 1**) to X/S and then multiplying by the mass of sulfur degassed (from melt inclusion and matrix glass sulfur concentrations[41 9 39,62]). This amount, in ppm, was added to the degassed lava composition to estimate an "un-degassed" magma composition c_i. It is possible that sulfide saturation could occur prior to melt inclusion entrapment, which would cap the sulfur concentration and deplete chalcophile metal concentrations in the melt inclusions; these processes would introduce error on these estimates. The arc basalts show no evidence for sulfide saturation; there are no sulfide globules in the melt inclusions from Ambrym[41], Stromboli and Etna[39], but Kīlauea and Holuhraun melt inclusions show occasional sulfide[62], although it is not clear whether these formed pre- or post-entrapment. We assume that sulfur is dominantly present as SO_2 in the gas plume and H_2S is neglected. It is also possible that under some circumstances S degasses from a larger volume of magma than metals/semi metals due to its lower solubility at higher pressures or mediation of metal degassing by halogen species. In order to overcome the difficulties associated with using *X*/*S* ratios to calculate ε_x, we repeat the calculation using *X*/*Cl* to calculate the pre-degassing metal (and semi-metal) concentrations for which data is available for most of the datasets used here (see **Supplementary Material**). We find there is good agreement between the ε_x calculated using *X*/*S* and *X*/*Cl* (see **Supplementary Material**).

Data Availability Statement

The authors declare that the data supporting the findings of this study, and the citations detailing data sources, are available within the article and its supplementary information files.

References

1 Nealson, K. H., Belz, A. & McKee, B. Breathing metals as a way of life: geobiology in action. *Antonie Van Leeuwenhoek* **81**, 215-222 (2002).

2 Graedel, T., Weschler, C. & Mandich, M. Influence of transition metal complexes on atmospheric droplet acidity. *Nature* **317**, 240 - 242 (1985).

3 Hedenquist, J. W. & Lowenstern, J. B. The role of magmas in the formation of hydrothermal ore deposits. *Nature* **370**, 519-527 (1994).

4 Williams-Jones, A. E. & Heinrich, C. A. 100th Anniversary special paper: vapor transport of metals and the formation of magmatic-hydrothermal ore deposits. *Economic Geology* **100**, 1287-1312 (2005).

5 Stoiber, R. E. & Rose, W. I. Fumarole incrustations at active Central American volcanoes. *Geochimica et Cosmochimica Acta* **38**, 495-516 (1974).

6 Allard, P. *et al*. Acid gas and metal emission rates during long‐lived basalt degassing at Stromboli volcano. *Geophysical Research Letters* **27**, 1207-1210 (2000).

7 Moune, S., Gauthier, P.-J. & Delmelle, P. Trace elements in the particulate phase of the plume of Masaya Volcano, Nicaragua. *Journal of Volcanology and Geothermal Research* **193**, 232-244 (2010).

8 Gauthier, P.-J. & Le Cloarec, M.-F. Variability of alkali and heavy metal fluxes released by Mt. Etna volcano, Sicily, between 1991 and 1995. *Journal of Volcanology and Geothermal Research* **81**, 311-326 (1998).

9 Gauthier, P. J., Sigmarsson, O., Gouhier, M., Haddadi, B. & Moune, S. Elevated gas flux and trace metal degassing from the 2014‐2015 fissure eruption at the Bárðarbunga volcanic system, Iceland. *Journal of Geophysical Research: Solid Earth* (2016).

10 Mather, T. *et al*. Halogens and trace metal emissions from the ongoing 2008 summit eruption of Kīlauea volcano, Hawaii. *Geochimica et cosmochimica acta* **83**, 292-323 (2012).

11 Hinkley, T. K., Lamothe, P. J., Wilson, S. A., Finnegan, D. L. & Gerlach, T. M. Metal emissions from Kilauea, and a suggested revision of the estimated worldwide metal output by quiescent degassing of volcanoes. *Earth and Planetary Science Letters* **170**, 315-325 (1999).

12 Aiuppa, A., Dongarrà, G., Valenza, M., Federico, C. & Pecoraino, G. Degassing of trace volatile metals during the 2001 eruption of Etna. *Volcanism and the Earth's atmosphere*, 41-54 (2003).

13 Hong, S., Candelone, J.-P., Soutif, M. & Boutron, C. F. A reconstruction of changes in copper production and copper emissions to the atmosphere during the past 7000 years. *Science of the total environment* **188**, 183-193 (1996).

14 Richards, J. P. Magmatic to hydrothermal metal fluxes in convergent and collided margins. *Ore Geology Reviews* **40**, 1-26 (2011).

15 Keith, M., Haase, K. M., Klemd, R., Schwarz-Schampera, U. & Franke, H. Systematic variations in magmatic sulphide chemistry from mid-ocean ridges, back-arc basins and island arcs. *Chemical Geology* (2016).

16 Jenner, F. E., O'Neill, H. S. C., Arculus, R. J. & Mavrogenes, J. A. The magnetite crisis in the evolution of arc-related magmas and the initial concentration of Au, Ag and Cu. *Journal of Petrology* **51**, 2445-2464 (2010).

17 Patten, C., Barnes, S.-J., Mathez, E. A. & Jenner, F. E. Partition coefficients of chalcophile elements between sulfide and silicate melts and the early crystallization history of sulfide liquid: LA-ICP-MS analysis of MORB sulfide droplets. *Chemical Geology* **358**, 170-188 (2013).

18 Hinkley, T. K., Le Cloarec, M.-F. & Lambert, G. Fractionation of families of major, minor, and trace metals across the melt-vapor interface in volcanic exhalations. *Geochimica et cosmochimica acta* **58**, 3255-3263 (1994).

19 Jenner, F. E. Cumulate causes for the low contents of sulfide-loving elements in the continental crust. *Nature Geoscience* **10**, 524 (2017).

20 Johnson, A. & Canil, D. The degassing behavior of Au, Tl, As, Pb, Re, Cd and Bi from silicate liquids: Experiments and applications. *Geochimica et Cosmochimica Acta* **75**, 1773-1784 (2011).

21 Kiseeva, E. S. & Wood, B. J. A simple model for chalcophile element partitioning between sulphide and silicate liquids with geochemical applications. *Earth and Planetary Science Letters* **383**, 68-81 (2013).

22 Heinrich, C., Günther, D., Audétat, A., Ulrich, T. & Frischknecht, R. Metal fractionation between magmatic brine and vapor, determined by microanalysis of fluid inclusions. *Geology* **27**, 755-758 (1999).

23 Botcharnikov, R. E. *et al*. Behavior of gold in a magma at sulfide-sulfate transition: Revisited. *American Mineralogist* **98**, 1459-1464 (2013).

24 Guo, H. & Audétat, A. Transfer of volatiles and metals from mafic to felsic magmas in composite magma chambers: An experimental study. *Geochimica et Cosmochimica Acta* **198**, 360-378 (2017).

25 Zajacz, Z., Candela, P. A., Piccoli, P. M. & Sanchez-Valle, C. The partitioning of sulfur and chlorine between andesite melts and magmatic volatiles and the exchange coefficients of major cations. *Geochimica et Cosmochimica Acta* **89**, 81-101 (2012).

26 Zajacz, Z., Candela, P. A., Piccoli, P. M., Wälle, M. & Sanchez-Valle, C. Gold and copper in volatile saturated mafic to intermediate magmas: Solubilities, partitioning,

and implications for ore deposit formation. *Geochimica et Cosmochimica Acta* **91**, 140-159 (2012).

27 Keppler, H. & Wyllie, P. J. Partitioning of Cu, Sn, Mo, W, U, and Th between melt and aqueous fluid in the systems haplogranite-H2O− HCl and haplogranite-H2O− HF. *Contr. Mineral. and Petrol.* **109**, 139-150 (1991).

28 Pennisi, M. & Le Cloarec, M. F. Variations of Cl, F, and S in Mount Etna's plume, Italy, between 1992 and 1995. *Journal of Geophysical Research: Solid Earth* **103**, 5061-5066 (1998).

29 Plank, T., Kelley, K. A., Zimmer, M. M., Hauri, E. H. & Wallace, P. J. Why do mafic arc magmas contain~ 4wt% water on average? *Earth and Planetary Science Letters* **364**, 168-179 (2013).

30 Wallace, P. J. Volatiles in subduction zone magmas: concentrations and fluxes based on melt inclusion and volcanic gas data. *Journal of Volcanology and Geothermal Research* **140**, 217-240 (2005).

31 Dixon, J. E. & Clague, D. A. Volatiles in Basaltic Glasses from Loihi Seamount, Hawaii: Evidence for a Relatively Dry Plume Component. *Journal of Petrology* **42**, 627-654, doi:10.1093/petrology/42.3.627 (2001).

32 Gerlach, T. M., McGee, K. A., Elias, T., Sutton, A. J. & Doukas, M. P. Carbon dioxide emission rate of Kīlauea Volcano: Implications for primary magma and the summit reservoir. *Journal of Geophysical Research: Solid Earth* **107**, 2189, doi:10.1029/2001JB000407 (2002).

33 Moore, G., Vennemann, T. & Carmichael, I. S. E. An empirical model for the solubility of H ₂ O in magmas to 3 kilobars. *American Mineralogist* **83**, 36-42, doi:10.2138/am-1998-1-203 (1998).

34 Gerlach, T. M. Exsolution of H2O, CO2, and S during eruptive episodes at Kīlauea Volcano, Hawaii. *Journal of Geophysical Research: Solid Earth* **91**, 12177-12185, doi:10.1029/JB091iB12p12177 (1986).

35 van Hinsberg, V., Berlo, K., Migdisov, A. & Williams-Jones, A. CO2-fluxing collapses metal mobility in magmatic vapour. *Geochemical Perspectives Letters* **824** (2016).

36 Li, C. & Ripley, E. M. Empirical equations to predict the sulfur content of mafic magmas at sulfide saturation and applications to magmatic sulfide deposits. *Mineralium Deposita* **40**, 218-230 (2005).

37 Liu, Y., Samaha, N.-T. & Baker, D. R. Sulfur concentration at sulfide saturation (SCSS) in magmatic silicate melts. *Geochimica et Cosmochimica Acta* **71**, 1783-1799 (2007).

38 Carroll, M. & Rutherford, M. Sulfide and sulfate saturation in hydrous silicate melts. *Journal of Geophysical Research: Solid Earth (1978–2012)* **90**, C601-C612 (1985).

39 Metrich, N. & Clocchiatti, R. Sulfur abundance and its speciation in oxidized alkaline melts. *Geochimica et Cosmochimica Acta* **60**, 4151-4160 (1996).

40 Jugo, P. J. Sulfur content at sulfide saturation in oxidized magmas. *Geology* **37**, 415-418 (2009).

41 Allard, P. *et al*. Prodigious emission rates and magma degassing budget of major, trace and radioactive volatile species from Ambrym basaltic volcano, Vanuatu island Arc. *Journal of Volcanology and Geothermal Research* (2016).

42 Gíslason, S. *et al*. Environmental pressure from the 2014–15 eruption of Bárðarbunga volcano, Iceland. *Geochem. Perspect. Lett* **1**, 84-93 (2015).

43 Wallace, P. J. & Carmichael, I. S. E. Sulfur in basaltic magmas. *Geochimica et Cosmochimica Acta* **56**, 1863-1874, doi:http://dx.doi.org/10.1016/0016-7037(92)90316-B (1992).

44 Richards, J. P. High Sr/Y arc magmas and porphyry Cu±Mo±Au deposits: just add water. *Economic Geology* **106**, 1075-1081 (2011).

45 Zajacz, Z., Halter, W. E., Pettke, T. & Guillong, M. Determination of fluid/melt partition coefficients by LA-ICPMS analysis of co-existing fluid and silicate melt inclusions: controls on element partitioning. *Geochimica et Cosmochimica Acta* **72**, 2169-2197 (2008).

46 Peach, C., Mathez, E. & Keays, R. Sulfide melt-silicate melt distribution coefficients for noble metals and other chalcophile elements as deduced from MORB: Implications for partial melting. *Geochimica et Cosmochimica Acta* **54**, 3379-3389 (1990).

47 Mungall, J. E., Brenan, J. M., Godel, B., Barnes, S. & Gaillard, F. Transport of metals and sulphur in magmas by flotation of sulphide melt on vapour bubbles. *Nature Geoscience* **8**, 216-219 (2015).

48 Le Vaillant, M., Barnes, S. J., Mungall, J. E. & Mungall, E. L. Role of degassing of the Noril'sk nickel deposits in the Permian–Triassic mass extinction event. *Proceedings of the National Academy of Sciences*, 201611086 (2017).

49 Larocque, A. C., Stimac, J. A., Keith, J. D. & Huminicki, M. A. Evidence for open-system behavior in immiscible Fe–S–O liquids in silicate magmas: implications for contributions of metals and sulfur to ore-forming fluids. *The Canadian Mineralogist* **38**, 1233-1249 (2000).

50 Nadeau, O., Williams-Jones, A. E. & Stix, J. Sulphide magma as a source of metals in arc-related magmatic hydrothermal ore fluids. *Nature Geoscience* **3**, 501-505 (2010).

51 Edmonds, M. & Liu, E. in *AGU Fall Meeting Abstracts*.

445 52 Hartley, M. E., Bali, E., Maclennan, J., Neave, D. A. & Halldórsson, S. A. Melt
446 inclusion constraints on petrogenesis of the 2014–2015 Holuhraun eruption, Iceland.
447 *Contr. Mineral. and Petrol.* **173**, 10 (2018).
448 53 Schmidt, M. E. & Grunder, A. L. Deep mafic roots to arc volcanoes: Mafic recharge
449 and differentiation of basaltic andesite at North Sister Volcano, Oregon Cascades.
450 *Journal of Petrology* **52**, 603-641 (2011).
451 54 Parmigiani, A., Faroughi, S., Huber, C., Bachmann, O. & Su, Y. Bubble accumulation
452 and its role in the evolution of magma reservoirs in the upper crust. *Nature* **532**, 492-
453 495 (2016).
454 55 Hattori, K. H. & Keith, J. D. Contribution of mafic melt to porphyry copper
455 mineralization: evidence from Mount Pinatubo, Philippines, and Bingham Canyon,
456 Utah, USA. *Mineralium Deposita* **36**, 799-806 (2001).
457 56 Evans, K.-A. & Tomkins, A.-G. The relationship between subduction zone redox
458 budget and arc magma fertility. *Earth and Planetary Science Letters* **308**, 401-409
459 (2011).
460 57 Goldfarb, R. J., Bradley, D. & Leach, D. L. Secular variation in economic geology.
461 *Economic Geology* **105**, 459-465 (2010).
462 58 Dupont, C. L., Butcher, A., Valas, R. E., Bourne, P. E. & Caetano-Anollés, G. History
463 of biological metal utilization inferred through phylogenomic analysis of protein
464 structures. *Proceedings of the National Academy of Sciences* **107**, 10567-10572
465 (2010).
466 59 Lambert, G., Le Cloarec, M., Ardouin, B. & Le Roulley, J. Volcanic emission of
467 radionuclides and magma dynamics. *Earth and Planetary Science Letters* **76**, 185-192
468 (1985).

60 Pennisi, M., Le Cloarec, M., Lambert, G. & Le Roulley, J. Fractionation of metals in volcanic emissions. *Earth and planetary science letters* **88**, 284-288 (1988).

61 Rubin, K. Degassing of metals and metalloids from erupting seamount and mid-ocean ridge volcanoes: Observations and predictions. *Geochimica et Cosmochimica Acta* **61**, 3525-3542 (1997).

62 Sides, I. R., Edmonds, M., Maclennan, J., Swanson, D. A. & Houghton, B. F. Eruption style at Kīlauea Volcano in Hawai`i linked to primary melt composition *Nature Geoscience* **7**, 464–469, doi:doi:10.1038/ngeo2140 (2014).

Correspondence and requests for materials should be addressed to Marie Edmonds (me201@cam.ac.uk).

Acknowledgements

We thank three anonymous reviewers for providing insightful comments on our manuscript, which improved it immensely. EJL is funded by a Leverhulme Early Career Fellowship.

Author contributions

All authors contributed equally to the concept and intellectual content of this article. ME took main responsibility for writing the article and for revising it after review.

Figures

Figure 1: **Metal systematics in the gas plumes of active basaltic volcanoes in a range of settings**. A: Metal fluxes in kg/day, with uncertainties, from four arc (or "arc affinity") volcanoes (blue) and two hotspot volcanoes (red)[6,7,9,10,12,41]. X/SO_2 for each dataset are shown

494 in **figure 1** of the **supplementary material**. B: Lava compositions (ppm) (a volcanic bomb
495 for Masaya; and scoria for Stromboli and Holuhraun) for the eruptions in each setting,
496 citations as above. Solid lines are degassed lava compositions; dashed lines show the metal
497 concentration prior to degassing (see **supplementary material** for data and methods). Note
498 that these dashed lines are only resolvable for some elements; for others the amount depleted
499 by degassing is relatively small. C: Enrichment factors relative to Cu for each volcano (see
500 Methods). Fields for each setting are shaded for ease of visual evaluation.
501
502 **Figure 2**: **Volcanic gas data compared to metal partitioning between silicate melt, sulfide**
503 **and aqueous fluid**. Emanation coefficients for the range of metals and semi-metals are
504 shown (see **methods** and **Supplementary Material**). Red shaded data are for volcanic gases
505 from hotspot volcanoes Kīlauea and Holuhraun (Iceland); blue shaded data are for volcanic
506 gases from arc basaltic eruptions Stromboli*, Etna, Masaya and Ambrym. Dark green
507 rectangles are sulfide-silicate melt partition coefficients and light green, aqueous fluid-melt
508 partition coefficients (see **Supplementary Material** for citations).
509 *Three emanation coefficients are shown for Stromboli (see Methods and Supplementary Material): 1. From[6]
510 calculated assuming $\varepsilon_{Pb} \sim 1\%$[59,60]; 2. calculated using plume X/SO_2 and the mass of sulfur degassed. 3. calculated
511 using plume X/Cl and the mass of chlorine degassed. Note that the X/SO_2 values for Etna aerosol
512 (**Supplementary Table 1**) are high compared with other arc volcanoes in this dataset and with other data from
513 Etna[8,28], which causes the emanation coefficients to be anomalously high when using this X/SO_2 ratio, combined
514 with the melt inclusion sulfur contents (see **methods**), to reconstruct the metal contents of the melts.
515
516 **Figure 3**: **Metal pathways through silicate melt, sulfide and aqueous fluid, and their**
517 **impact on the metal composition of basaltic volcanic gas and aerosol.** We envisage
518 Kīlauea and Holuhraun to correspond to the far left case, where much of the magmatic water
519 exsolves at low pressures in the crust, coinciding with late stage sulfide saturation. Arc basalts

correspond to the far right case, where deep magmatic aqueous fluid phase saturation occurs with no sulfide saturation, allowing metal-rich aqueous fluid to form.

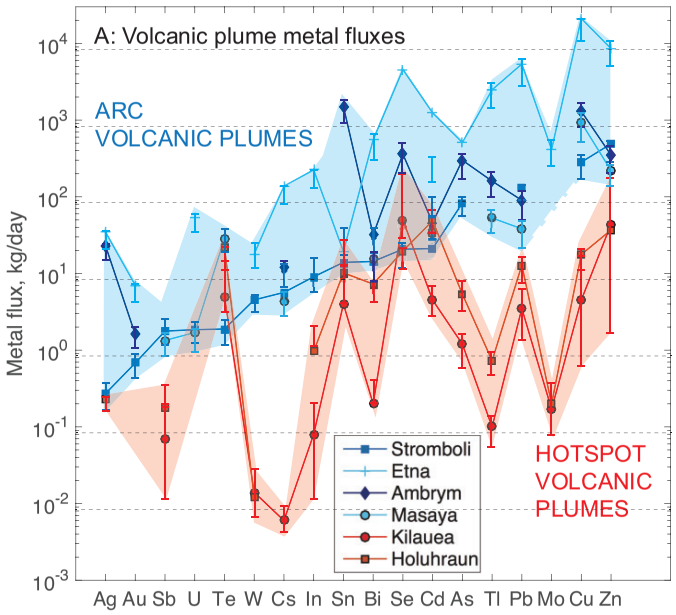
A: Volcanic plume metal fluxes
ARC
VOLCANIC PLUMES
HOTSPOT
VOLCANIC
PLUMES
Stromboli
Etna
Ambrym
Masaya
Kilauea
Holuhraun
Metal flux, kg/day
Ag Au Sb U Te W Cs In Sn Bi Se Cd As Tl Pb Mo Cu Zn

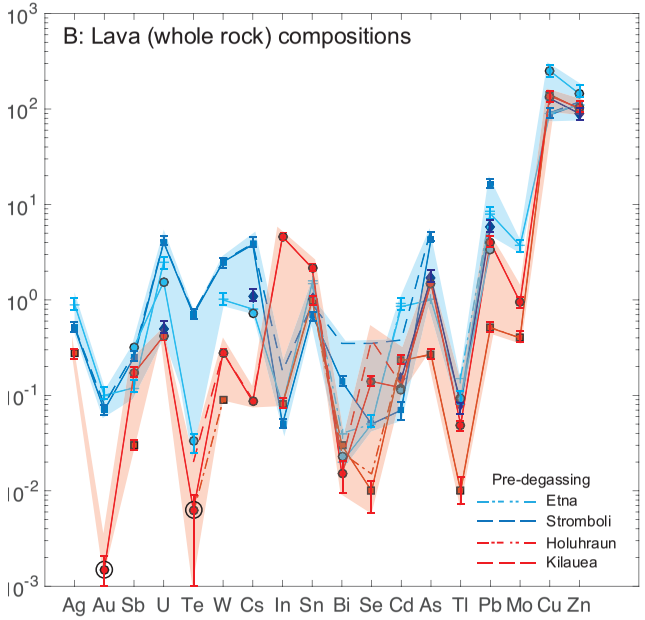
B: Lava (whole rock) compositions
Pre-degassing
Etna
Stromboli
Holuhraun
Kilauea
Ag Au Sb U Te W Cs In Sn Bi Se Cd As Tl Pb Mo Cu Zn

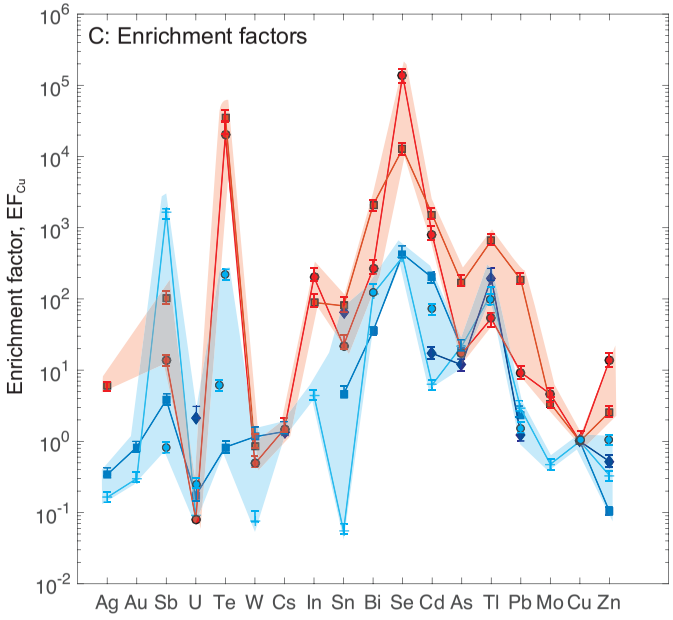
C: Enrichment factors
Enrichment factor, EF$_{Cu}$
Ag Au Sb U Te W Cs In Sn Bi Se Cd As Tl Pb Mo Cu Zn

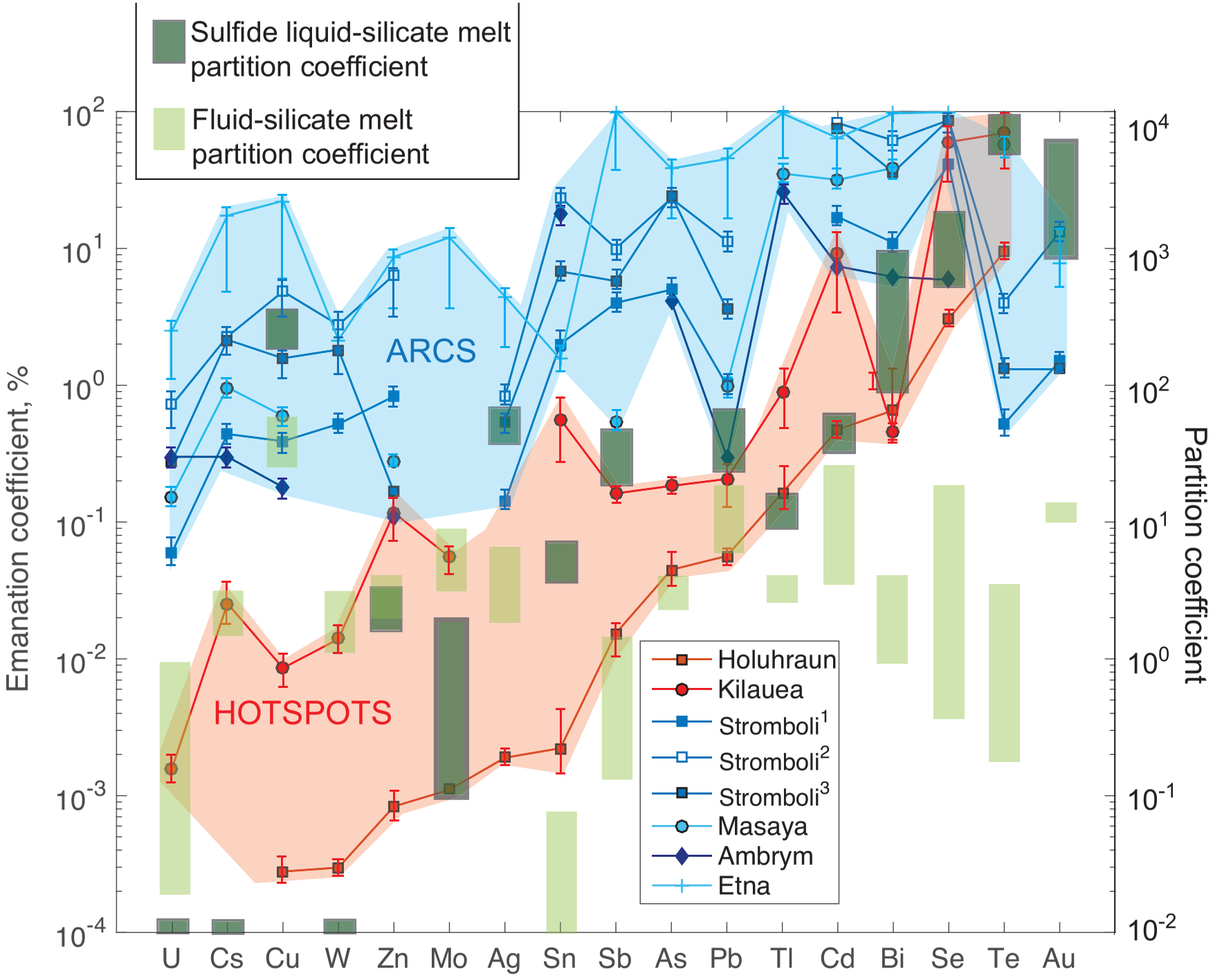
Sulfide liquid-silicate melt partition coefficient
Fluid-silicate melt partition coefficient
ARCS
HOTSPOTS
Holuhraun
Kilauea
Stromboli1
Stromboli2
Stromboli3
Masaya
Ambrym
Etna
Emanation coefficient, %
Partition coefficient
U
Cs
Cu
W
Zn
Mo
Ag
Sn
Sb
As
Pb
Tl
Cd
Bi
Se
Te
Au

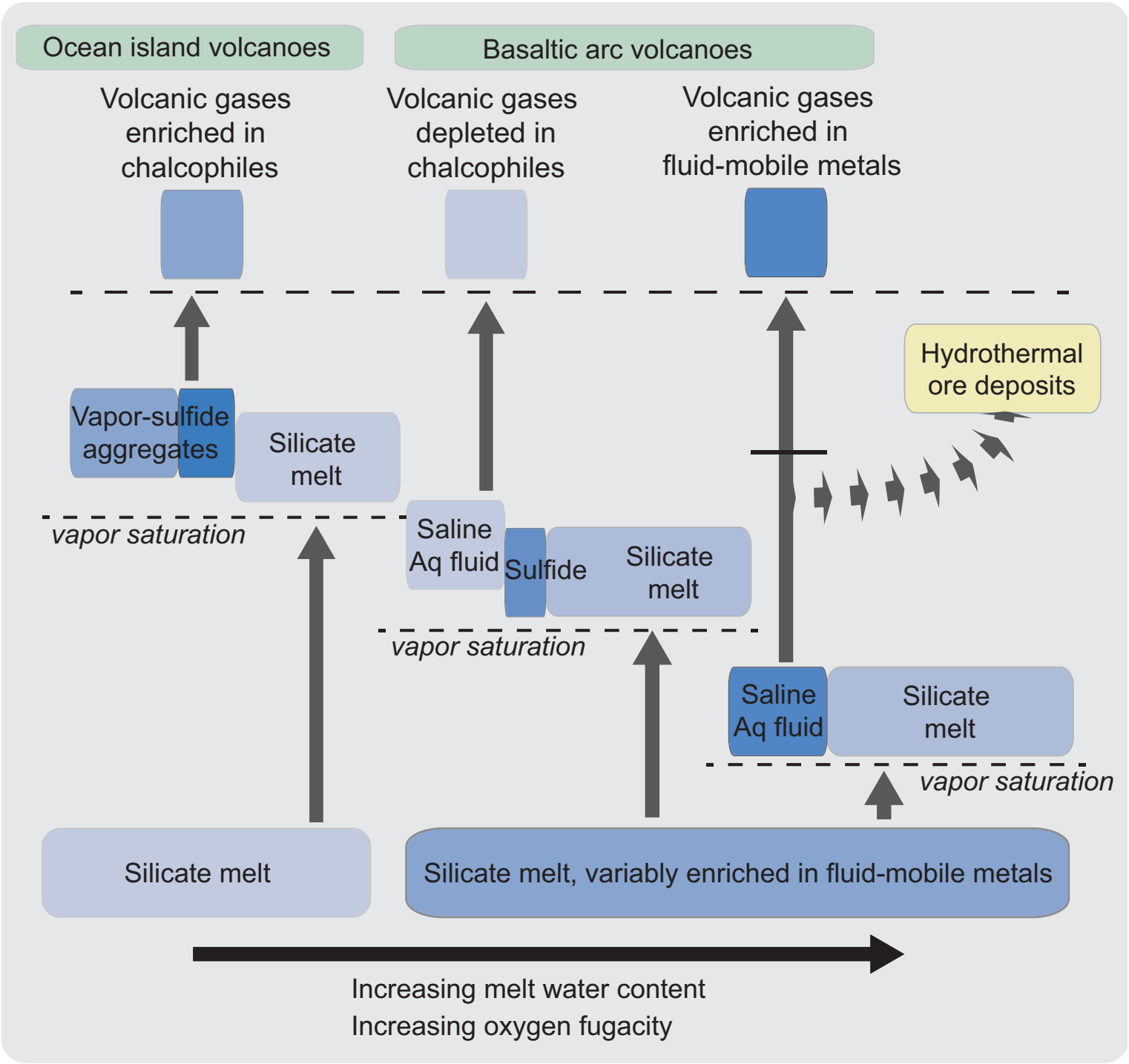
Ocean island volcanoes
Basaltic arc volcanoes
Volcanic gases enriched in chalcophiles
Volcanic gases depleted in chalcophiles
Volcanic gases enriched in fluid-mobile metals
Hydrothermal ore deposits
Vapor-sulfide aggregates
Silicate melt
vapor saturation
Saline Aq fluid
Sulfide
Silicate melt
vapor saturation
Saline Aq fluid
Silicate melt
vapor saturation
Silicate melt
Silicate melt, variably enriched in fluid-mobile metals
Increasing melt water content
Increasing oxygen fugacity

Supplementary Material

Tracking metal pathways in magmas using volcanic gas fingerprints

M. Edmonds, T. A. Mather, E. J. Liu

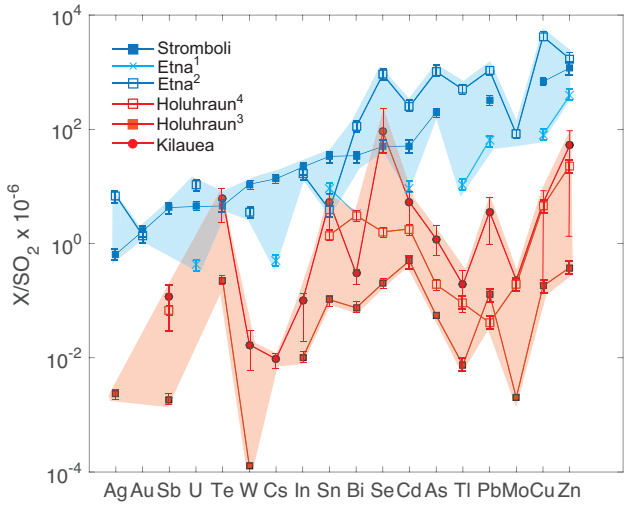

Supplementary figure 1: Ratios X/SO_2, in mg/kg, in the gas plumes volcanoes from arc (blue) and ocean island settings (red). Volcanoes are Stromboli (solid blue squares), Etna (light blue crosses[1] and blue open squares[2]), Kīlauea (red circles) and Holuhraun, Iceland (red squares[3] and open squares[4]). Elements are ordered using the Stromboli dataset, as **Figure 1** of the main paper. See **table 1** for citations and errors on data.

Contribution of metals to the volcanic plume as silicate ash particles

Volcanic particulates sampled by filter packs in plumes are made up of both aerosols (aqueous liquids with dissolved acid gases into which metals partition from high temperature magmatic vapor, before being condensed upon quenching in the atmosphere) and also silicate particles, fragments of bubble walls typically launched into the plume by bubble bursting. The bulk analysis of the particulate fraction then inevitably results in some of the metal budget being sourced from the silicate particles rather than metals that have been volatilized from the magma forming the aerosol and gas phases. This effect is most significant for the less mobile, more lithophile elements, and less important for the more volatile metals, with high vapor-melt partition coefficients. Here we discuss the magnitude of this effect.

At Stromboli a minor silicate contribution was inferred for Cr, Cs, Cu, Rb and W (0-5%), but a significant one for Te and Zn (10%) and corrected accordingly[3]. For Etna, it has been noted that significant concentrations of Al, Si, Na, K, and REE are present in the plume, which must be sourced from silicate material[2]. Elements such as Se, Cd and Sb, however, which are present only in trace amounts in silicate melts, are present in significant quantities in filter pack analyses (greater than more abundant lithophile trace elements such as Th, Sc), suggesting that these metals are volatile. The weight ash fraction (WAF) was calculated by these authors[2] using the abundance of REE. The calculated WAF is very low for Bi (0.1%), Sb (0.2%), Se and Tl (both 0.1%); slightly more significant for Pb (3%), As (2%) and Cu (6%) but significant for Mo, Zn, Te and W (33, 25, 59, 100% respectively), although Te is poorly constrained by its low abundance (close to detection, table 1) in lavas. There is abundant evidence from elsewhere that Te is highly volatile[4]. Another study used Th abundance to calculate the proportion contributed from ash and derived considerably lower estimates: zero for Tl, Bi, Cd; then 3% for Cu, 1% for Sn, 2% for Zn and 0.5% for Pb[1]. At Ambrym negligible ash contributions were inferred for Ag, Au, Sn, Bi, Se, Cd, As, Tl, with a slightly larger contribution for Cs (0-15%), Pb (~2%), Cu (0-17%) and Zn (7-40%)[5]. For Holuhraun the concentrations of Th and REE were used to estimate very low proportion of silicate ash (about 10 µg of ash per filter on average) and therefore the effect of ash contamination was neglected[6]. An ash correction was not calculated for the Kīlauea dataset.

Solid sulfides, oxides, halides, and oxyhydroxides might also be present in the plume, given the dramatic fall in solubility of gaseous metal chloride, sulfide and other species during the drop in temperature from the basalt liquidus temperature to ambient conditions. The presence of these phases may impact the estimation of silicate ash fraction because even nominally "immobile" high field strength elements like Sn, Th or REE may have significant volatility in the presence of abundant gaseous F, as is well known from studies of greisen-forming ore-bearing hydrothermal systems e.g.[7].

We conclude that while in some cases up to 40% of a metal or semi-metal species might be supplied from ash, in general the metals we plot here are highly volatile and their abundance is controlled dominantly by transport initially in the magmatic vapor phase and later (at and away from the vent) in liquid aerosol.

Metal-carrying capacity of magmatic vapor phase at low pressures

Experimental studies[8] and thermodynamic modeling have shown that metals form stable complexes with chloride, sulfate and fluoride in volcanic plumes[9]. Volcanic gas at the surface is the low density phase which is the result of separation of a brine phase from a saline supercritical fluid as it decompresses and cools (**supplementary figure 2**). Up to now, much of the literature on metals in volcanic environments has been gleaned from condensates[10,11], deposited during shallow cooling of magmatic fluids, which have little relevance to the question of how mafic volcanic systems outgas metals to the atmosphere[12]. Little data exists for hot magmatic plumes outgassed directly from the magma column during eruptions, which are expected to contain a far higher load of metals dispersed into the atmosphere, either as gas or as sub micron-aerosols, owing to their higher temperature and chloride content[13,14].

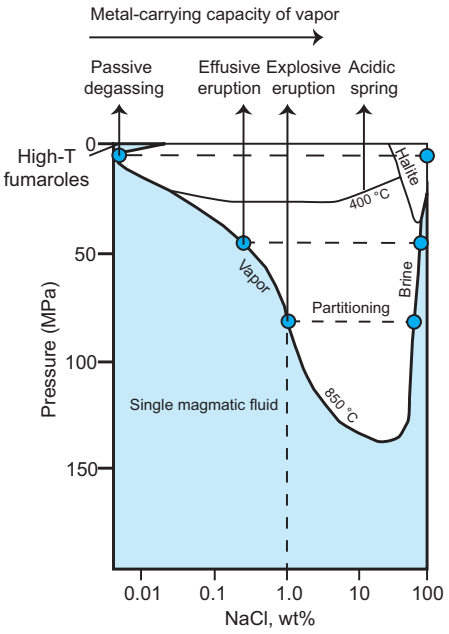

Supplementary figure 2: NaCl-H_2O phase diagram plotted in pressure-composition space, modified after[15].

The solvus will shrink significantly at high temperatures, increasing the salinity and metal-carrying capacity of outgassing vapor. It is possible that supercritical metal-rich fluids may reach the surface, avoiding immiscibility. Until recently[16,17], it was assumed by some authors that low salinity volcanic gas would not have the capacity to dissolve large quantities of metals as chloride complexes, and the brine phase was therefore the favored ore-forming medium[18]. **Figure 1 (main paper)** shows that, on the contrary, volcanic gases are highly significant carriers of metals.

Table 1, below, shows the data used in this paper and its sources. We focus here on active basaltic volcanoes with data acquired using filter packs at the vent (*i.e.* not from fumaroles or lava flows, or as condensates and sublimates).

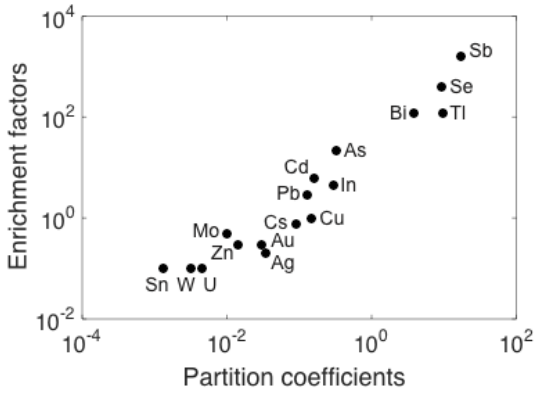

Supplementary Figure 3: Enrichment factors from **table 1** for elements in the plume of Etna (Italy), using Cu as a normalising element, plotted against "absolute" partition coefficients (defined as mass of element in the gas/mass of element in the melt phase) calculated by estimating a dilution factor for the plume[12].

Table 1: Metal/semi-metals contents of degassed lavas and gas/aerosol samples; X/SO_2, metal fluxes, volatilities and enrichment factors for the datasets presented in the main paper.

Erupted lava metal content, in ppm. Data sources: Stromboli Volcano (Italy)[3], Holuhraun (Iceland)[6], Etna (Italy)[2], Ambrym Volcano (Vanuatu)[5], Kīlauea (Hawaii, USA), standard BHVO[19] and Masaya Volcano (Nicaragua)[20]. Error typically <10% for ICP-MS, IMA with internal calibration using standards.

Gas and aerosol metal data, in $\mu g/m^3$, from Stromboli Volcano (Italy)[3], Holuhraun (Iceland)[6], Etna (Italy)[1], Ambrym Volcano (Vanuatu)[5], Kīlauea Volcano (Hawaii, USA)[14] and Masaya Volcano (Nicaragua)[20]. Uncertainties are shown in brackets for each element within each dataset and are typically 5-25%.

Flux of element *X* in kg per day, calculated using the mass ratio *X/SO₂** and the independently measured flux of SO_2 (data sources as above). The uncertainty on the flux measurement is 30-32%, propagated from errors on SO_2 flux (~30%) and errors on gas and aerosol measurements (5-10%).

* *X/SO₂,* in mg/kg; errors on *X/SO₂* are propagated from errors on analysis of S and X in gas/aerosol phase and including, where available[21], the standard deviation of repeat analyses on the same day, amounting to 7-17% for the former and up to 95% for the latter[21].

Emanation coefficient, ε_x, is calculated as the percentage of the metal *x* that has degassed from the silicate melt, equal to: $\varepsilon_x = \left(c_i - c_f\right) / c_i$, where c_i is the initial concentration of element x in the magma and c_f is the final concentration of element *x* in the post-eruptive lava (as originally defined by[22]. The *emanation coefficients* given are estimated in a range of ways (which are indicated as footnotes for each sub-table). The *emanation coefficient* ε_x of these elements from the magma can be assessed from their mean enrichment factor (EF) and the emanation coefficient of Pb from molten basalt (which may be assumed to be constant at 0.01[23]), as[1,3,24]: $\varepsilon_x^{-1} = 1 + \left[\left(EF_{Pb} / EF_x\right)\left(1 - \varepsilon_{Pb}\right) / \varepsilon_{Pb}\right]$. We also calculate the concentration of metals and semi-metals in the silicate melt prior to degassing, c_i. The amount of metal (or semi-metal) in the gas plume was "added" back into to the degassed lava composition by converting the mass X/SO_2 ratio in the plume and then multiplying by the pre-eruptive melt concentration of sulfur (from melt inclusion concentrations, corrected for matrix glass sulfur concentration[5 6 25,26]). This amount, in ppm, was added to the degassed lava composition to estimate a "un-degassed" magma composition c_i. For some datasets we also calculate emanation coefficients using *X/Cl* to estimate pre-degassing metal concentrations in the melt, using melt inclusion and matrix glass concentrations as shown in the footnotes. Errors on the *emanation coefficients* are propagated from typical errors on the individual electron microprobe analyses of sulfur, which is typically 5%, and errors on X/SO_2. Total errors

EF_{Cu} is the *enrichment factor* relative to copper (Cu), equal to $EF_{Cu} = \left(\frac{[X]}{[Cu]}\right)_{gas} \Big/ \left(\frac{[X]}{[Cu]}\right)_{lava}$. Errors are propagated from the individual metal analyses and range from 14-17%.

Note on propagation of errors: X/SO_2, enrichment factors and emanation coefficients are calculated using the measured concentration data as defined above, with individual errors as defined in the paper sources (see tables below). Errors on these quantities are propagated from the error on the individual measurements, where the uncertainty on quantity z (which is a function of independent variables x and y e.g. z = xy, or z = x/y) is the sum of the squares of the fractional errors, or error percentages, of x and y: $\frac{\delta z}{z}\sqrt{\left(\frac{\delta x}{x}\right)^2 + \left(\frac{\delta y}{y}\right)^2}$.

Volcano	**Stromboli**[3]								
Elements	*Lava, ppm*	*Gas, aerosol, $\mu g/m^3$*	*Flux, kg/day*	*X/SO_2, mg/kg*	*X/Cl, mg/kg*	*Emanation coefficient ε (%)*[a]	*Emanation coefficient ε (%)*[b]	*Emanation coefficient ε (%)*[c]	*EF_{Cu}*
S	40	4540 (±227)	4.15×10^5 ($\pm 1.26 \times 10^5$)			98	99	98	
Cl	550	2910 (±146)	1.40×10^5 ($\pm 4.25 \times 10^4$)			74	79	71	
Ag	0.51	6.0×10^{-3} (±0.0003)	0.27 (±0.08)	0.65 (±0.05)	2.06 (±0.22)	0.14	0.82	0.54	0.3 (±0.045)
Au	0.07	2.0×10^{-3} ($\pm 2.0 \times 10^{-4}$)	0.68 (±0.22)	1.64 (±0.18)	0.69 (±0.08)	1.5	13	1.3	0.8 (±0.14)
Sb	0.25	3.3×10^{-2} ($\pm 3.3 \times 10^{-3}$)	1.77 (±0.56)	4.27 (±0.48)	11.3 (±1.2)	4	10	5.8	3.8 (±0.65)
U	4.0	2.4×10^{-2} ($\pm 1.2 \times 10^{-3}$)	1.85 (±0.56)	4.45 (±0.31)	8.25 (±0.90)	0.06	0.72	0.28	0.2 (±0.03)
Te	0.7	2.0×10^{-2} ($\pm 1.0 \times 10^{-3}$)	1.89 (±0.57)	4.55 (±0.32)	6.87 (±0.76)	0.52	4.1	1.3	0.8 (±0.12)
W	2.5	1.0×10^{-1} ($\pm 1.0 \times 10^{-2}$)	4.53 (±1.43)	10.9 (±1.22)	34.4 (±3.8)	0.52	2.8	1.8	1.2 (±0.21)
Cs	3.8	1.8×10^{-1} ($\pm 1.8 \times 10^{-2}$)	5.66 (±1.79)	13.6 (±1.52)	61.9 (±6.8)	0.44	2.3	2.2	1.4 (±0.24)
Sn	0.70	1.1×10^{-1} ($\pm 5.5 \times 10^{-3}$)	14.0 (±4.26)	33.6 (±2.38)	37.8 (±4.2)	2.0	24	6.8	4.6 (±0.69)
Bi	0.14	1.7×10^{-1} ($\pm 8.5 \times 10^{-3}$)	14.3 (±4.35)	34.5 (±2.44)	58.4 (±6.4)	11	62	36	35.2 (±5.3)
Se	0.05	7.4×10^{-1} ($\pm 7.4 \times 10^{-2}$)	20.8 (±6.58)	50.0 (±5.59)	254 (±28)	41	87	87	429 (±74)
Cd	0.07	4.8×10^{-1} ($\pm 2.4 \times 10^{-2}$)	21.1 (±6.42)	50.9 (±3.60)	165 (±18)	17	83	76	199 (±30)
As	4.30	3.0 (±0.3)	83.0 (±26.3)	200 (±22.4)	1030 (±110)	5	23	24	20.2 (±3.5)
Tl									
Pb	16.2	1.3 (±0.065)	132 (±40.2)	318 (±22.5)	447 (±49)	1	11	3.6	2.3 (±0.35)
Mo									
Cu	87	3.0 (±0.15)	283 (±86.1)	682 (±48.2)	1030 (±110)	0.39	4.8	1.6	1.0 (±0.15)
Zn	112	0.40 (±0.04)	491 (±155)	1180 (±132)	137 (±15)	0.83	6.4	0.17	0.1 (±0.017)

[a] *Emanation coefficient* calculated assuming $\varepsilon_{Pb} \sim 1\%$[22,23] (see table caption), from[3].
[b] *Emanation coefficient* calculated using plume *X/SO_2* and the mass of sulfur degassed (from matrix and melt inclusion glass analysis; see table caption and methods). Melt inclusion and matrix glass data from[3,27] (0.34 and 0.004 wt% sulfur).
[c] *Emanation coefficient* calculated using plume *X/Cl* and the mass of chlorine degassed (from matrix and melt inclusion glass analysis; see table caption and methods). Melt inclusion and matrix glass data from[3,27] (0.19 and 0.055 wt% chlorine).

Volcano	**Holuhraun**[6]						
Elements	*Lava ppm*	*Gas, aerosol*[a] *μg/m³*	*Flux, kg/day*	*X/SO₂ mg/kg*	*Emanation coefficient ε (%)*[b]	*Emanation coefficient ε (%)*[c]	*EF$_{Cu}$*
S	400[28]	185 (±19)				74	500 (±85)
Cl		3.64 (±0.36)		1.97×10^4 ($\pm 2.2 \times 10^3$)		32	42 (±7.1)
Ag	0.28	1.54×10^{-3} ($\pm 1.5 \times 10^{-4}$)	0.23 (±0.04)	2.41×10^{-3} ($\pm 2.7 \times 10^{-4}$)	1.8×10^{-3}	1.9×10^{-3}	5.9 (±1.0)
Au							
Sb	0.026	2.47×10^{-3} ($\pm 2.5 \times 10^{-4}$)	0.18 (±0.06)	1.82×10^{-3} ($\pm 2.0 \times 10^{-4}$)	1.5×10^{-2}	1.5×10^{-2}	103 (±18)
U							
Te	0.0048	1.58×10^{-1} ($\pm 1.6 \times 10^{-2}$)	22.3 (±7.1)	2.28×10^{-1} ($\pm 2.5 \times 10^{-2}$)	9.2	9.5	35800 (±6200)
W	0.093	7.30×10^{-5} ($\pm 7.3 \times 10^{-6}$)	1.2×10^{-2} ($\pm 3.8 \times 10^{-3}$)	1.26×10^{-4} ($\pm 1.0 \times 10^{-5}$)	2.9×10^{-4}	3.0×10^{-4}	0.9 (±0.16)
Cs							
Sn	0.99	7.28×10^{-2} ($\pm 7.3 \times 10^{-3}$)	10.2 (±3.2)	1.04×10^{-1} ($\pm 1.1 \times 10^{-2}$)	2.2×10^{-2}	2.2×10^{-2}	80.0 (±14)
Bi	0.025	4.80×10^{-2} ($\pm 4.8 \times 10^{-3}$)	7.28 (±2.3)	7.5×10^{-2} ($\pm 8.4 \times 10^{-3}$)	6.4×10^{-1}	6.6×10^{-1}	2080 (±360)
Se	0.014	1.68×10^{-1} ($\pm 1.7 \times 10^{-2}$)	19.6 (±6.2)	2.01×10^{-1} ($\pm 2.2 \times 10^{-2}$)	2.9	3.1	12800 (±2200)
Cd	0.23	3.30×10^{-1} ($\pm 3.3 \times 10^{-2}$)	48.7 (±15.4)	4.99×10^{-1} ($\pm 5.6 \times 10^{-2}$)	4.5×10^{-1}	4.8×10^{-1}	1540 (±270)
As	0.27	4.09×10^{-2} ($\pm 4.1 \times 10^{-3}$)	5.38 (±1.7)	5.50×10^{-2} ($\pm 6.2 \times 10^{-3}$)	4.4×10^{-2}	4.5×10^{-2}	167 (±30)
Tl	0.01	6.07×10^{-3} ($\pm 6.1 \times 10^{-4}$)	0.73 (±0.23)	7.46×10^{-3} ($\pm 8.3 \times 10^{-4}$)	1.6×10^{-1}	1.6×10^{-1}	658 (±114)
Pb	0.51	8.79×10^{-2} ($\pm 8.8 \times 10^{-3}$)	12.8 (±4.1)	1.31×10^{-1} ($\pm 1.5 \times 10^{-2}$)	5.4×10^{-2}	5.7×10^{-2}	186 (±32)
Mo	0.40	1.26×10^{-3} ($\pm 1.3 \times 10^{-4}$)	0.2 (±0.06)	2.01×10^{-3} ($\pm 2.2 \times 10^{-4}$)	1.1×10^{-3}	1.1×10^{-3}	3.4 (±0.6)
Cu	142	1.30×10^{-1} ($\pm 1.3 \times 10^{-2}$)	17.7 (±5.6)	1.80×10^{-1} ($\pm 2.0 \times 10^{-2}$)	2.7×10^{-4}	2.8×10^{-4}	1.0 (±0.2)
Zn	100	2.37×10^{-1} ($\pm 2.4 \times 10^{-2}$)	36.9 (±11.7)	3.79×10^{-1} ($\pm 4.2 \times 10^{-2}$)	8.0×10^{-4}	8.3×10^{-4}	2.6 (±0.5)

[a] sample name BAR-A from[6]

[b] *Emanation coefficient* (expressed in terms of a %) from[6], calculated using a dilution factor (calculated using at-vent and downwind plume sulfur dioxide concentrations). Error propagated from gas measurements are in the range 10-20%.

[c] *Emanation coefficient* calculated assuming the degassing of 1100 ppm sulfur, from 1500 ppm to 400 ppm[28] and using the X/SO_2 ratio of the plume to reconstruct the concentration of element X prior to degassing.

Volcano	**Etna**[2]							
	Lava	*Gas, aerosol*[a]	*Flux,*	*X/SO_2*[e]*,*	*Emanation coefficient*	*Emanation coefficient*	*Emanation coefficient*	*EF_{Cu}*
	ppm	*$\mu g/m^3$*	*kg/day*	*mg/kg*	*ε (%)*[b]	*ε (%)*[c]	*ε (%)*[d]	
Elements:								
S	150	181 (±19)	5.0×10^6 ($\pm 1.7 \times 10^6$)					71 (±9)
Cl	1700	67 (±7)	9.2×10^5 ($\pm 3.0 \times 10^5$)	1.85×10^5 ($\pm 2.0 \times 10^4$)	39.9	56.4	0.80	2.3 (±0.3)
Ag	0.9	2.5×10^{-3} ($\pm 2.5 \times 10^{-4}$)	35 (±12)	6.91 (±0.77)	4.47	8.36	0.07	0.2 (±0.035)
Au	0.1	5.1×10^{-4} ($\pm 5.1 \times 10^{-5}$)	7.0 (±2.3)	1.41 (±0.16)	7.91	14.3	0.10	0.3 (±0.05)
Sb	0.12	3.32 (±0.33)	4.5×10^4 (±1.5)	9.17×10^3 ($\pm 1.0 \times 10^3$)	99.8	99.9	85	1630 (±282)
U	2.5	3.8×10^{-3} ($\pm 3.8 \times 10^{-4}$)	52.5 (±17.3)	10.5 (±1.2)	2.50	4.75	0.035	0.1 (±0.012)
Te								
W	1	1.3×10^{-3} ($\pm 1.3 \times 10^{-4}$)	18.0 (±5.94)	3.59 (±0.4)	2.14	4.09	0.035	0.1 (±0.017)
Cs	0.8	0.01 (±0.001)	138 (±46)	27.6 (±3.1)	17.4	29.1	0.26	0.74 (±0.13)
Sn	1.5	1.4×10^{-3} ($\pm 1.4 \times 10^{-4}$)	19.3 (±6.8)	3.87 (±0.43)	1.55	2.97	0.035	0.1 (±0.017)
Bi	0.02	4.0×10^{-2} ($\pm 4.0 \times 10^{-3}$)	552 (±182)	110 (±12)	97.1	98.5	29	118 (±20.4)
Se	0.05	3.3×10^{-1} ($\pm 3.3 \times 10^{-2}$)	4560 (±1500)	912 (±101)	99.1	99.5	58	388 (±67.2)
Cd	0.85	9.0×10^{-2} ($\pm 9.0 \times 10^{-3}$)	1243 (±435)	249 (±27)	64.1	77.7	2.1	6.2 (±1.1)
As	1	3.7×10^{-2} ($\pm 3.7 \times 10^{-3}$)	511 (±179)	102 (±11)	38.4	54.9	7.12	22 (±3.8)
Tl	0.09	1.8×10^{-1} ($\pm 1.8 \times 10^{-2}$)	2486 (±870)	497 (±55)	97.1	98.5	29	118 (±20.4)
Pb	8	3.9×10^{-1} ($\pm 3.9 \times 10^{-2}$)	5387 (±1890)	1077 (±120)	45.1	61.5	1.0	2.9 (±0.50)
Mo	3.7	3.0×10^{-2} ($\pm 3.0 \times 10^{-3}$)	414 (±145)	82.9 (±9.2)	12.0	21.0	0.17	0.5 (±0.09)
Cu	90	1.53 (±0.15)	2.11×10^4 ($\pm 7.4 \times 10^3$)	4227 (±470)	22.3	35.8	0.35	1.0 (±0.17)
Zn	110	6.2×10^{-1} (±0.062)	8564 (±3000)	1710 (±1.90)	8.67	15.6	0.10	0.3 (±0.05)

[a] ET1 of[2]

[b] *Emanation coefficient* calculated using plume *X/SO_2* and the mass of sulfur degassed (from matrix and melt inclusion glass analysis; see table caption and methods). Melt inclusion and matrix glass data from (0.32 and 0.015 wt% sulfur)[26].

[c] *Emanation coefficient* calculated using plume *X/Cl* and the mass of chlorine degassed (from matrix and melt inclusion glass analysis; see table caption and methods). Melt inclusion and matrix glass data from (0.28 and 0.17 wt% chlorine)[26].

[d] *Emanation coefficient* calculated assuming $\varepsilon_{Pb} \sim 1\%$[22,23] (see table caption and methods).

[e] Note that these X/SO_2 values are high compared with other arc volcanoes in this dataset and with other data from Etna[1,29], which causes the emanation coefficients to be anomalously high when using the X/SO_2 ratio, combined with the melt inclusion sulfur contents, to reconstruct the metal contents of the melts (main paper, **figure 2**).

Volcano	**Masaya**[20] *Lava ppm*	*Gas, aerosol, $\mu g/m^3$*	*X/SO_2, mg/kg*	*Flux, kg/day*	*EF_{Cu}*
Elements					
S	150	0.11 (±0.006)	5.0×10^5 [30] ($\pm 6.0 \times 10^4$)	5.0×10^5 ($\pm 1.65 \times 10^4$)	2.8×10^3 ($\pm 0.4 \times 10^3$)
Cl					
Ag					
Au					
Sb	0.321	0.0074 (±0.00074)	0.35 (±0.04)	0.18 (±0.06)	0.92 (±0.12)
U	1.55	0.01 (±0.001)	0.48 (±0.05)	0.24 (±1.2)	0.26 (±0.034)
Te	0.033	0.19 (± 0.019)	9.0 (±1.0)	4.5 (±1.5)	230 (±29)
W					
Cs	0.711	0.029 (±0.0029)	1.38 (±0.15)	0.69 (±0.23)	1.6 (±0.21)
In					
Sn					
Bi	0.023	0.061 (±0.006)	2.90 (±0.32)	1.5 (±0.5)	110 (±14)
Se					
Cd	0.113	0.22 (±0.022)	20.9 (±2.3)	11 (±3.6)	77 (±10)
As					
Tl	0.092	0.21 (±0.021)	20.0 (±2.2)	10 (±3.4)	91 (±12)
Pb	3.36	0.142 (±0.014)	13.5 (±1.5)	6.7 (±2.2)	1.7 (±0.22)
Mo					
Cu	251	6.32 (±0.063)	600 (±67)	300 (±99)	1.0 (±0.33)
Zn	144	1.69 (±0.17)	160 (±18)	80 (±26)	0.47 (±0.06)

Volcano	**Kīlauea**								
	Lava[19]	*Gas, aerosol*[14]	*Flux,*	*X/SO$_2$*	*X/Cl*	*Emanation coefficient ε (%)*[a]	*Emanation coefficient ε (%)*[b]	*Emanation coefficient ε (%)*[c]	*EF$_{Cu}$*
	ppm	*μg/m^3*	*kg/day*	*mg/kg*	*mg/kg*				
Elements:									
S		120 (±13)	7×10^8 [14] ($\pm 65 \times 10^6$)			89	89	44	
Cl	402	16 (±1.5)	448 (±45)	640 (±45)		0.42	30	3.3	
Ag	3.32×10^{-1}								
Au	1.5×10^{-3}								
Sb	1.7×10^{-1}	2.5×10^{-3} ($\pm 0.4 \times 10^{-4}$)	0.07 (±0.06)	0.12 (±0.01)	1.6×10^2 (±20)	0.16	0.22	1.46	13.7 (±2.1)
U	4.2×10^{-1}	3.6×10^{-5} ($\pm 5.0 \times 10^{-6}$)		0.0029 ($\pm 3 \times 10^{-4}$)	2.3 (±0.3)	0.0016	0.16	0.0087	0.080 (±0.02)
Te	6.3×10^{-3}	1.34×10^{-1} ($\pm 1.5 \times 10^{-2}$)	4.8 (±3.0)	6.3 (±0.7)	8.4×10^3 ($\pm 1 \times 10^3$)	70	99	96	1.98×10^4 ($\pm 3.8 \times 10^3$)
W	2.80×10^{-1}	1.46×10^{-4} ($\pm 2.6 \times 10^{-5}$)	1.4×10^{-2} ($\pm 8.0 \times 10^{-3}$)	0.017 ($\pm 2 \times 10^{-3}$)	9.1 (±1.3)	0.014	0.97	0.053	4.86×10^{-1} (±0.11)
Cs	8.6×10^{-2}	1.38×10^{-4} ($\pm 3.0 \times 10^{-5}$)	6.0×10^{-3} ($\pm 2.0 \times 10^{-3}$)	9.5×10^{-3} ($\pm 1 \times 10^{-3}$)	8.6 (±1.3)	0.025	2.92	0.16	1.50 (±0.4)
In	4.6	1.00×10^{-3} ($\pm 1.0 \times 10^{-4}$)	8.0×10^{-2} ($\pm 7.0 \times 10^{-2}$)	0.1 ($\pm 1 \times 10^{-2}$)	63 (±10)	0.0050	0.41	18	202 (±37)
Sn	2.15	5.1×10^{-2} ($\pm 9.0 \times 10^{-3}$)	4.5 (± 2.3)	5.3 ($\pm 6 \times 10^{-1}$)	3.2×10^3 ($\pm 5 \times 10^2$)	0.56	31	2.3	22.1 (±5.2)
Bi	1.5×10^{-1}	4.3×10^{-3} ($\pm 1.9 \times 10^{-4}$)	0.21 (±0.07)	0.3 ($\pm 3 \times 10^{-2}$)	2.7×10^2 (±40)	0.46	35	22	267 (±43)
Se	1.4×10^{-1}	1.49 (±0.15)	62.5 (±45)	91 (±10)	9.3×10^4 ($\pm 1 \times 10^4$)	60	99	99	1.39×10^5 ($\pm 2.5 \times 10^4$)
Cd	1.2×10^{-1}	1.03×10^{-1} ($\pm 1.2 \times 10^{-2}$)	3.8 (±2.3)	5.3 (±0.6)	6.4×10^3 ($\pm 1 \times 10^3$)	9.2	94	46	800 (±150)
As	1.5	2.73×10^{-2} ($\pm 2.0 \times 10^{-3}$)	1.1 (±0.5)	1.2 (±0.1)	1.7×10^3 ($\pm 3 \times 10^3$)	0.18	25.4	1.8	17.0 (±2.9)
Tl	4.9×10^{-2}	2.8×10^{-3} ($\pm 0.4 \times 10^{-3}$)	0.13 (±0.07)	0.19 (±0.02)	1.8×10^2 (±30)	0.88	52	5.5	53.3 (±11)
Pb	4.0	4.0×10^{-2} ($\pm 0.3 \times 10^{-2}$)	3.1 (±2.3)	3.6 (±0.4)	2.5×10^3 (±400)	0.21	16	1	9.32 (±1.6)
Mo	9.50×10^{-1}	4.7×10^{-3} ($\pm 0.5 \times 10^{-3}$)	1.7×10^{-1} (±0.1)	0.23 (±0.03)	2.9×10^2 (±50)	0.056	8.5	0.50	4.61 (±0.86)
Cu	137	1.5×10^{-1} ($\pm 9.0 \times 10^{-3}$)	4.5 (±4.0)	5.1 (±0.06)	9.4×10^3 ($\pm 1.5 \times 10^3$)	0.0086	2.0	0.11	1.00 (±0.16)
Zn	102	1.50 (±0.17)	45 (±44)	52 (±6)	9.4×10^4 ($\pm 1.3 \times 10^4$)	0.12	22	1.5	13.7 (±2.6)

[a] *Emanation coefficient* calculated using plume *X/SO$_2$* and the mass of sulfur degassed (from matrix and melt inclusion glass analysis; see table caption and methods). Melt inclusion and matrix glass data: 0.13 and 0.015 wt% sulfur[31].
[b] *Emanation coefficient* calculated using plume *X/Cl* and the mass of chlorine degassed (from matrix and melt inclusion glass analysis; see table caption and methods). Melt inclusion and matrix glass data: 0.05 and 0.035 wt% chlorine[25]. Note that the uncertainty on this emanation coefficient is high owing to the low concentration of Cl in the plume and the uncertainty associated with estimating the chlorine budget from melt inclusions and matrix glasses[21,32].
[c] *Emanation coefficient* calculated assuming $\varepsilon_{Pb} \sim 1\%$[22,23] (see table caption and methods).

Volcano	**Ambrym**[5]				
	Lava[5], *ppm*	*Gas, aerosol*[5], *μg/m*^{3}	*Flux, kg/day*	*Emanation coefficient ε (%)*[a]	EF_{Cu}
Elements					
S	0.015			95	
Cl	0.07			30	
Ag		3.20 (±0.19)	23 (±4.0)		
Au		3.1×10^{-3} ($\pm 1.9 \times 10^{-4}$)	1.6 (±0.5)		
Sb					
U	0.5	1.3×10^{-2} ($\pm 5.2 \times 10^{-4}$)		0.3	2.1 (±0.33)
Te					
W					
Cs	1.1	1.8×10^{-2} ($\pm 1.1 \times 10^{-3}$)	12 (±3.7)	0.3	1.3 (±0.21)
Sn	1	0.8 (±0.08)	1500 (±470)	18	64.5 (±11.8)
Bi		4.1×10^{-2} ($\pm 1.6 \times 10^{-3}$)	32 (±9.7)	6.2	
Se		3.1×10^{-1} (±0.03)	360 (±114)	5.9	
Cd	0.15	3.2×10^{-2} ($\pm 3.2 \times 10^{-3}$)	46 (±15)	7.4	17.2 (±3.2)
As	1.7	0.25 (±0.025)	300 (±95)	4.1	11.9 (±2.2)
Tl	0.08	0.195 (±0.012)	160 (±49.0)	26	197 (±32.4)
Pb	5.9	0.09 (±0.004)	90 (±27)	0.3	1.2 (±0.19)
Mo					
Cu	129.00	1.60 (±0.10)	1300 (±400)	0.18	1.00 (±0.16)
Zn	89.5	0.58 (±0.035)	350 (±110)	0.11	0.52 (±0.086)

[a] *Emanation coefficient* calculated using measurements of ε_{Pb} from[5] (see table caption and methods).

Comparison of different ways to calculate emanation coefficients

The tables above show various different ways to estimate the emanation coefficient, defined as $\varepsilon_x = \left(c_i - c_f\right) \Big/ c_i$, where c_i is the initial concentration of element *x* in the magma and c_f is the final concentration of element *x* in the post-eruptive lava (as originally defined by[22]). The plots shown in **supplementary figure 4** show how they compare to one another. The emanation coefficients calculated using the various methods are broadly consistent with one another in terms of order of volatility, with the methods using X/SO_2 and *X/Cl* to "add back" metals in the proportions given by these ratios to calculate c_i and thus emanation coefficient yielding higher emanation coefficients than the methods based on measurement of the emanation coefficient of ^{210}Pb[23], by 1-20 times.

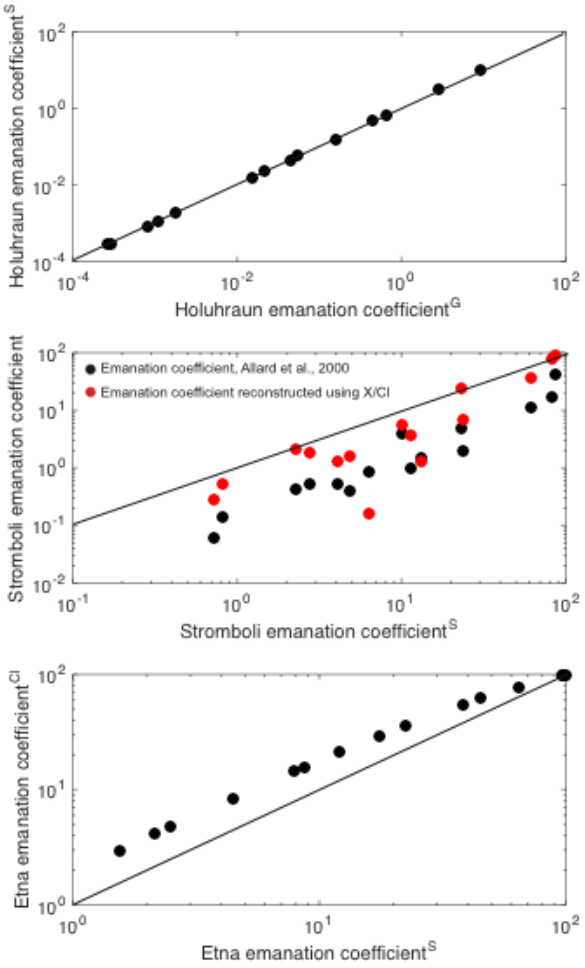

Supplementary Figure 4: top: emanation coefficient for metals and semi-metals from Holuhraun calculated by[6] by using a dilution factor calculated from their measurements of sulfur in vent and plume gases (x axis) versus emanation coefficient calculated in this study using the mass of sulfur outgassed from melt (from melt inclusion and matrix glass microanalysis[28]) and X/SO_2 ratios in the plume) to calculate c_i (y axis). Middle: emanation coefficient for Stromboli metals and semi-metals calculated in this study using X/SO_2 to reconstruct c_i (x axis) plotted versus emanation coefficient from[3] using measurements of the emanation coefficient of ^{210}Pb[23] (black); and using *X/Cl* (this study) to calculate c_i (red) (see table caption and methods for detail). Bottom: comparison between emanation coefficient calculated using X/SO_2 (x axis) with that calculated using *X/Cl* (y axis) to calculate c_i for Mt Etna (Italy). Black solid line is the 1:1 line.

Metal partition coefficients

Table 2: Vapor-melt ($D_{vapor\text{-}melt}$) and sulfide-silicate melt ($D_{sulfide\text{-}silicate\ melt}$) partition coefficients used in this paper. Sources are shown either in column header or in individual cells.

	$D_{vapor\text{-}melt}$ [33]	$D_{vapor\text{-}melt}$	$D_{sulfide\text{-}silicate\ melt}$	$D_{sulfide\text{-}silicate\ melt}$ [34]	$D_{sulfide\text{-}silicate\ melt}$ [35]
U		0.002 to 0.45[36]	0.001[37]		
Cs	2.3 to 5.9	0.5 to 10[38]			
W	1.8 to 4.5	3 to 16[39]		0.003 to 0.1	
Cu	33 to 70	1 to 80[40]	260 to 447[41]	540 to 1040	1042 to 1624
Zn	2.3 to 5	9 to 70	1.9 to 3.1[41]	0.28 to 0.94	2.4 to 4.7
Mo	5.5 to 9.8	9.3 to 523[39]		0.1 to 2.58	
Ag	1.9 to 7	7 to 10[38]	360 to 617[41]	300 to 700	853 to 1528
Sn		0.002 to 0.078[40]		2.4 to 6.0	9 to 13
Sb	0.14 to 2.6	1 to 10[38]	15 to 34[41]	1.4 to 11.2	
As	3 to 6.2	1 to 2.5[42]		0.3 to 19.7	
Pb	8.4 to 15	2 to 14[39]	26 to 54[41]	13 to 48	45 to 71
Tl	3.1 to 6	3.5 to 12.4[39]	10 to 17[41]		
Cd	6.5 to 30		45 to 82[41]		61 to 193
Bi	1 to 5.3	7 to 30[38]		110 to 1130	
Se	0.59 to 12		790 to 1500[41]		
Au		12 to 15[42]		930 to 5500	
Te	0.22 to 6.7		6000 to 16000[41]		

Notes on experimental conditions.

[33] Partitioning of metals between vapor and basalt silicate melt at 850 °C, 2 kbar, Cl- and H_2O-bearing fluids.

[34] Partitioning between basanite melt, sulfide liquid and monosulfide solid solution, at 1175 to 1300 °C, 1.5-3.0 GPa, 3 units below to 1 unit above FMQ buffer, relevant to mantle conditions.

[35] Mid-ocean ridge basalts at FMQ to FMQ-1.

[36] Haplogranite melt composition, aqueous fluid with HCl and HF, 2 kbar, 750 C.

[37] 1-10 GPa, 1750–2100 °C, 0–28 wt% S, and fO_2 2 log units below IW (core conditions).

[38] Granitic and peralkaline melts, melts with high chlorinities (1-14 mole/kg), $\log fO_2$ = NNO−1.7 to NNO+4.5.

[39] Haplogranite melt composition, with H_2O-HCl and H_2O-HF vapor phase. For Cu, lowest $D_{vapor\text{-}melt}$ for H_2O-only and highest for Cl-rich case; for Sn highest $D_{vapor\text{-}melt}$ for Cl-rich case, but poorly constrained.

[40] Haplogranite melt composition, aqueous fluid with HCl and HF, 2 kbar, 750 C.

[41] The silicate constituent was either a MORB or a composition close to the 1.5 GPa eutectic composition in the system anorthite–diopside–forsterite ($An_{50}Di_{28}Fo_{22}$). FeO was added to vary FeO activity.

References

1 Gauthier, P.-J. & Le Cloarec, M.-F. Variability of alkali and heavy metal fluxes released by Mt. Etna volcano, Sicily, between 1991 and 1995. *Journal of Volcanology and Geothermal Research* **81**, 311-326 (1998).

2 Aiuppa, A., Dongarrà, G., Valenza, M., Federico, C. & Pecoraino, G. Degassing of trace volatile metals during the 2001 eruption of Etna. *Volcanism and the Earth's atmosphere*, 41-54 (2003).

3 Allard, P. *et al.* Acid gas and metal emission rates during long-lived basalt degassing at Stromboli volcano. *Geophysical Research Letters* **27**, 1207-1210 (2000).

4 Saunders, J. A. & Brueseke, M. E. Volatility of Se and Te during subduction-related distillation and the geochemistry of epithermal ores of the western United States. *Economic Geology* **107**, 165-172 (2012).

5 Allard, P. *et al.* Prodigious emission rates and magma degassing budget of major, trace and radioactive volatile species from Ambrym basaltic volcano, Vanuatu island Arc. *Journal of Volcanology and Geothermal Research* (2016).

6 Gauthier, P. J., Sigmarsson, O., Gouhier, M., Haddadi, B. & Moune, S. Elevated gas flux and trace metal degassing from the 2014-2015 fissure eruption at the Bárðarbunga volcanic system, Iceland. *Journal of Geophysical Research: Solid Earth* (2016).

7 Gysi, A. P. & Williams-Jones, A. E. Hydrothermal mobilization of pegmatite-hosted REE and Zr at Strange Lake, Canada: A reaction path model. *Geochimica et Cosmochimica Acta* **122**, 324-352 (2013).

8 Webster, J., Holloway, J. & Hervig, R. Partitioning of lithophile trace elements between H 2 O and H 2 O+ CO 2 fluids and topaz rhyolite melt. *Economic Geology* **84**, 116-134 (1989).

9 Symonds, R. B., Rose, W. I., Reed, M. H., Lichte, F. E. & Finnegan, D. L. Volatilization, transport and sublimation of metallic and non-metallic elements in high temperature gases at Merapi Volcano, Indonesia. *Geochimica et Cosmochimica Acta* **51**, 2083-2101 (1987).

10 Stoiber, R. E. & Rose, W. I. Fumarole incrustations at active Central American volcanoes. *Geochimica et Cosmochimica Acta* **38**, 495-516 (1974).

11 Buat-Ménard, P. & Arnold, M. The heavy metal chemistry of atmospheric rarticulate matter emitted by Mount Etna Volcano. *Geophysical Research Letters* **5**, 245-248 (1978).

12 Mather, T. A. Volcanoes and the environment: Lessons for understanding Earth's past and future from studies of present-day volcanic emissions. *Journal of Volcanology and Geothermal Research* **304**, 160-179 (2015).

13 Mather, T., Pyle, D. & Oppenheimer, C. Tropospheric volcanic aerosol. *Volcanism and the Earth's Atmosphere*, 189-212 (2003).

14 Mather, T. *et al.* Halogens and trace metal emissions from the ongoing 2008 summit eruption of Kīlauea volcano, Hawaii. *Geochimica et Cosmochimica Acta* **83**, 292-323 (2012).

15 Hedenquist, J. W. & Lowenstern, J. B. The role of magmas in the formation of hydrothermal ore deposits. *Nature* **370**, 519-527 (1994).

16 Heinrich, C. A., Ryan, C. G., Mernagh, T. P. & Eadington, P. J. Segregation of ore metals between magmatic brine and vapor; a fluid inclusion study using PIXE microanalysis. *Economic Geology* **87**, 1566-1583 (1992).

17 Zajacz, Z. & Halter, W. Copper transport by high temperature, sulfur-rich magmatic vapor: Evidence from silicate melt and vapor inclusions in a basaltic andesite from the Villarrica volcano (Chile). *Earth and Planetary Science Letters* **282**, 115-121 (2009).

18 Williams, T. J., Candela, P. A. & Piccoli, P. M. The partitioning of copper between silicate melts and two-phase aqueous fluids: an experimental investigation at 1 kbar, 800 C and 0.5 kbar, 850 C. *Contr. Mineral. and Petrol.* **121**, 388-399 (1995).

19 Gladney, E. & Goode, W. Elemental concentrations in eight new United States Geological Survey rock standards: a review. *Geostandards newsletter* **5**, 31-64 (1981).
20 Moune, S., Gauthier, P.-J. & Delmelle, P. Trace elements in the particulate phase of the plume of Masaya Volcano, Nicaragua. *Journal of Volcanology and Geothermal Research* **193**, 232-244 (2010).
21 Mather, T. A. *et al.* Halogens and trace metal emissions from the ongoing 2008 summit eruption of Kīlauea volcano, Hawai`i. *Geochimica et Cosmochimica Acta* **83**, 292-323, doi:http://dx.doi.org/10.1016/j.gca.2011.11.029 (2012).
22 Lambert, G., Le Cloarec, M., Ardouin, B. & Le Roulley, J. Volcanic emission of radionuclides and magma dynamics. *Earth and Planetary Science Letters* **76**, 185-192 (1985).
23 Pennisi, M., Le Cloarec, M., Lambert, G. & Le Roulley, J. Fractionation of metals in volcanic emissions. *Earth and planetary science letters* **88**, 284-288 (1988).
24 Rubin, K. Degassing of metals and metalloids from erupting seamount and mid-ocean ridge volcanoes: Observations and predictions. *Geochimica et Cosmochimica Acta* **61**, 3525-3542 (1997).
25 Sides, I. R., Edmonds, M., Maclennan, J., Swanson, D. A. & Houghton, B. F. Eruption style at Kīlauea Volcano in Hawai`i linked to primary melt composition *Nature Geoscience* **7**, 464–469, doi:doi:10.1038/ngeo2140 (2014).
26 Metrich, N. & Clocchiatti, R. Sulfur abundance and its speciation in oxidized alkaline melts. *Geochimica et Cosmochimica Acta* **60**, 4151-4160 (1996).
27 Bertagnini, A., Métrich, N., Landi, P. & Rosi, M. Stromboli volcano (Aeolian Archipelago, Italy): An open window on the deep-feeding system of a steady state basaltic volcano. *Journal of Geophysical Research: Solid Earth* **108** (2003).
28 Hartley, M. E., Bali, E., Maclennan, J., Neave, D. A. & Halldórsson, S. A. Melt inclusion constraints on petrogenesis of the 2014–2015 Holuhraun eruption, Iceland. *Contr. Mineral. and Petrol.* **173**, 10 (2018).
29 Pennisi, M. & Le Cloarec, M. F. Variations of Cl, F, and S in Mount Etna's plume, Italy, between 1992 and 1995. *Journal of Geophysical Research: Solid Earth* **103**, 5061-5066 (1998).
30 Williams-Jones, G., Rymer, H. & Rothery, D. A. Gravity changes and passive SO2 degassing at the Masaya caldera complex, Nicaragua. *Journal of Volcanology and Geothermal Research* **123**, 137-160 (2003).
31 Edmonds, M., Sides, I. R. & Maclennan, J. Insights into mixing, fractionation and degassing of primitive melts at Kīlauea Volcano, Hawai`i. *AGU Monograph* (2014).
32 Edmonds, M., Gerlach, T. M. & Herd, R. A. Halogen degassing during ascent and eruption of water-poor basaltic magma. *Chemical Geology* **263**, 122-130, doi:http://dx.doi.org/10.1016/j.chemgeo.2008.09.022 (2009).
33 Guo, H. & Audétat, A. Transfer of volatiles and metals from mafic to felsic magmas in composite magma chambers: An experimental study. *Geochimica et Cosmochimica Acta* **198**, 360-378 (2017).
34 Li, Y. & Audétat, A. Partitioning of V, Mn, Co, Ni, Cu, Zn, As, Mo, Ag, Sn, Sb, W, Au, Pb, and Bi between sulfide phases and hydrous basanite melt at upper mantle conditions. *Earth and Planetary Science Letters* **355**, 327-340 (2012).
35 Patten, C., Barnes, S.-J., Mathez, E. A. & Jenner, F. E. Partition coefficients of chalcophile elements between sulfide and silicate melts and the early crystallization history of sulfide liquid: LA-ICP-MS analysis of MORB sulfide droplets. *Chemical Geology* **358**, 170-188 (2013).
36 Keppler, H. & Wyllie, P. J. Role of fluids in transport and fractionation of uranium and thorium in magmatic processes. *Nature* **348**, 531 (1990).

37 Wheeler, K. T., Walker, D., Fei, Y., Minarik, W. G. & McDonough, W. F. Experimental partitioning of uranium between liquid iron sulfide and liquid silicate: Implications for radioactivity in the Earth's core. *Geochimica et Cosmochimica Acta* **70**, 1537-1547 (2006).

38 Zajacz, Z., Halter, W. E., Pettke, T. & Guillong, M. Determination of fluid/melt partition coefficients by LA-ICPMS analysis of co-existing fluid and silicate melt inclusions: controls on element partitioning. *Geochimica et Cosmochimica Acta* **72**, 2169-2197 (2008).

39 MacKenzie, J. M. & Canil, D. Fluid/melt partitioning of Re, Mo, W, Tl and Pb in the system haplobasalt-H 2 O-Cl and the volcanic degassing of trace metals. *Journal of Volcanology and Geothermal Research* **204**, 57-65 (2011).

40 Keppler, H. & Wyllie, P. J. Partitioning of Cu, Sn, Mo, W, U, and Th between melt and aqueous fluid in the systems haplogranite-H2O− HCl and haplogranite-H2O− HF. *Contr. Mineral. and Petrol.* **109**, 139-150 (1991).

41 Kiseeva, E. S. & Wood, B. J. A simple model for chalcophile element partitioning between sulphide and silicate liquids with geochemical applications. *Earth and Planetary Science Letters* **383**, 68-81 (2013).

42 Simon, A. C., Pettke, T., Candela, P. A., Piccoli, P. M. & Heinrich, C. A. The partitioning behavior of As and Au in S-free and S-bearing magmatic assemblages. *Geochimica et Cosmochimica Acta* **71**, 1764-1782 (2007).